Bioactive Materials 47 (2025) 136–151

Contents lists available at ScienceDirect

Bioactive Materials

journal homepage: www.keaipublishing.com/en/journals/bioactive-materials

Cartilage structure-inspired nanofiber-hydrogel composite with robust proliferation and stable chondral lineage-specific differentiation function to orchestrate cartilage regeneration for artificial tracheal construction

Yaqiang Li [a,1], Xiaowei Xun [b,1], Liang Duan [a,1], Erji Gao [a,1], Jiaxin Li [d], Lei Lin [a], Xinping Li [f], Aijuan He [e,**], Haiyong Ao [b,***], Yong Xu [a,c,****], Huitang Xia [g,h,*]

[a] Department of Thoracic Surgery, Shanghai Pulmonary Hospital, Tongji University School of Medicine, Shanghai, 200430, China
[b] School of Materials Science and Engineering, East China Jiaotong University, Nanchang, 330013, China
[c] Department of Plastic Surgery, The First Affiliated Hospital of Shandong First Medical University & Shandong Provincial Qianfoshan Hospital, Jinan, 250014, China
[d] Department of Pharmacy, Jiangxi University of Chinese Medicine, Nanchang, 330004, China
[e] Department of Facial Plastic and Reconstructive Surgery, Eye & ENT Hospital of Fudan University, Shanghai, 200031, China
[f] Department of Thyroid Center, Shanghai Tongji Hospital, Tongji University School of Medicine, Shanghai, 200065, China
[g] Department of Neurosurgery, The First Affiliated Hospital of Shandong First Medical University & Shandong Provincial Qianfoshan Hospital, Jinan, 250014, China
[h] Jinan Clinical Research Center for Tissue Engineering Skin Regeneration and Wound Repair, Jinan, Shandong, 250014, China

ARTICLE INFO

Keywords:
Cartilage tissue engineering
Hydrogel
Bacterial cellulose
Growth factor
Tissue-engineered trachea

ABSTRACT

Tissue engineering strategies hold promise for constructing biomimetic tracheal substitutes to repair circumferential tracheal defects. However, current strategies for constructing off-the-shelf cartilage analogs for artificial trachea grafts face challenges of chondrocyte scarcity and inadequate culture strategies, which require extensive cell expansion and prolonged *in vitro* culture to generate robust neo-cartilage. To address these issues, we developed a nanofiber-hydrogel composite with superior mechanical performance by incorporating fragment oxidized bacterial cellulose (BC) nanofibers into a gelatin methacryloyl (GelMA) hydrogel network. Additionally, a biomaterial system was developed based on this composite, featuring dual-release functionality of fibroblast growth factor (FGF) and transforming growth factor beta (TGF-β) to facilitate step-wise maturation of neo-cartilage tissue. This process includes early-stage proliferation followed by second-stage extracellular matrix (ECM) deposition, driving the transition from proliferation to chondrogenesis. By encapsulating chondrocytes within the biomaterial system, mature neo-cartilage tissues with typical cartilage lacunae structures and abundant homogeneous cartilage-specific ECM deposition were successfully regenerated *in vitro* and *in vivo*. Furthermore, with a tailor-made growth factor-releasing strategy, the biomaterial system with low cell seeding density achieved biochemically and biomechanically functional neo-cartilage tissue regeneration, comparable to that achieved with high cell seeding density in the nanofiber-hydrogel composite. Based on the current biomaterial system, mature and functional cartilage-ring analogs were successfully constructed and applied to repair tracheal defects. Overall, the biomaterial system developed in this study provides a promising strategy for engineering transplantable, high-quality cartilage substitutes, with translational potential for artificial trachea construction.

* Corresponding author. Department of Neurosurgery, The First Affiliated Hospital of Shandong First Medical University & Shandong Provincial Qianfoshan Hospital, Jinan, 250014, China.
** Corresponding author.
*** Corresponding author.
**** Corresponding author. Department of Thoracic Surgery, Shanghai Pulmonary Hospital, Tongji University School of Medicine, Shanghai, 200430, China.
E-mail addresses: heaijuan2013@163.com (A. He), aohyong@126.com (H. Ao), xuyong@tongji.edu.cn (Y. Xu), xiahuitang@163.com (H. Xia).
[1] These authors contributed equally to this work.

https://doi.org/10.1016/j.bioactmat.2025.01.007
Received 10 September 2024; Received in revised form 6 January 2025; Accepted 7 January 2025

1. Introduction

Tracheal reconstruction surgery is commonly required for circumferential tracheal defects caused by tracheal injury, benign tracheal stenosis, or tracheal tumors [1]. However, primary end-to-end anastomosis is not feasible when circumferential tracheal defects account for more than 50 % of the tracheal length in adults or 30 % in infants [2]. Therefore, there is a need to construct an ideal artificial tracheal substitute for treating long-segment tracheal injuries. Several types of tracheal grafts have been used to provide airway conduits, including artificial prostheses, decellularized tracheas, and tissue-engineered tracheal constructs [3,4]. As a tissue-derived graft, the decellularized tracheal graft has long been considered the most effective method; however, donor tissue availability and immunogenicity limit its application. In contrast, synthetic tissue-engineered trachea grafts (TETG) have immense potential to provide an "off-the-shelf" substitute for tracheal replacement [5]. Moreover, preparing a tracheal cartilage component with excellent mechanical support to maintain airway patency is an essential prerequisite for constructing a TETG [6].

Owing to their good biocompatibility, tunable mechanical properties, and three-dimensional (3D) polymeric networks, hydrogels have been widely used to encapsulate cells and construct tracheal cartilage analogs. Particularly, gelatin methacryloyl (GelMA) hydrogels have been widely used in cartilage tissue engineering because their properties resemble those of the natural extracellular matrix (ECM) [7]. However, the weak mechanical strength of GelMA hydrogel makes it unsuitable for load-bearing cartilage replacements. The suboptimal mechanical properties of hydrogels necessitate prolonged *in vitro* culture to generate primary cartilaginous tissues with adequate mechanical performance to maintain morphological fidelity and structural stability [8]. Native cartilage can be regarded as highly hydrated hydrogel tissue with a frame structure based on collagen nanofibers. The superior mechanical properties of natural cartilage tissue are intrinsically related to its distinctive physiological structure. However, most current hydrogels only resemble the non-fibrous part of the native cartilage ECM [9]. It can be presumed that the lack of a nanofiber network resembling native collagen compromises the mechanical properties of the hydrogel. Previous studies have successfully incorporated nanofibrillated cellulose (NFC) into alginate hydrogels as reinforcing fibers to enhance their structural integrity and mechanical performance, validating the above hypothesis [10]. Therefore, introducing a nanofiber structure can greatly improve the mechanical properties of GelMA hydrogels, holding the possibility to achieve the rapid construction of artificial tracheal cartilage substitutes for subsequent *in vivo* transplantation [11].

Although nanofiber-reinforced hydrogels exhibit satisfactory mechanical properties, achieving robust chondrocyte proliferation and stable lineage function in a 3D hydrogel culture environment to form high-quality, homogeneous cartilaginous tissue remains an unmet goal in cartilage tissue engineering [12]. Improved regeneration of cartilaginous tissues based on the current hydrogel system still relies on a high input of chondrocytes and an extended period of chondrogenic induction [13]. Thus, developing a tailor-made strategy to maximize the potential of a limited number of chondrocytes for the regeneration of functional cartilage tissue is essential. Previous studies have shown that a combination of different growth factors, especially transforming growth factor beta (TGF-β) and fibroblast growth factor (FGF), can reduce the doubling time of proliferated chondrocytes and shorten the maturation stage for chondral lineage-specific differentiation [14,15]. However, current bioengineering strategies selectively supplement exogenous cytokines during *in vitro* culture processes to accelerate chondrocyte expansion or tissue maturation without precisely regulating cell behavior with growth factors at different stages of cartilage tissue regeneration [14]. A fully defined, tailor-made culture strategy is needed for the generation of high-quality tracheal cartilaginous grafts based on a cartilage-inspired nanofiber-GelMA hydrogel composite.

Bacterial cellulose (BC), as a natural nanofiber material, possesses exceptional mechanical strength and biocompatibility and has been successfully applied in cartilage tissue engineering in our previous studies [16,17]. Therefore, BC nanofibers have the potential to serve as the fibrous component of nanofiber-hydrogel composites. However, the chemical inertness and nonbiodegradability of BC greatly limit its application in tissue engineering. In recent years, various oxidation modification methods have been used to improve the degradability and surface functionalization of BC, paving the way for the use of BC nanofibers to enhance hydrogel properties [18]. In addition, oxidized BC (OBC) nanofibers contain aldehyde functional groups, which help for loading the biofunctional compounds on the surface of OBC nanofibers and realizing the controllable release. Therefore, incorporating OBC nanofibers into hydrogels promises enhanced mechanical properties and the development of new culture strategies.

In this study, we developed a novel bioengineering strategy to construct a nanofiber-hydrogel composite with robust proliferation and stable lineage function for tissue-engineered tracheal cartilage regeneration (Scheme 1). The introduction of OBC nanofibers not only significantly improved the mechanical properties of GelMA hydrogels but also facilitated the precise orchestration of cell programs through sequential growth factor release. Chondrocyte proliferation, chondral-lineage differentiation, and ECM production within the nanofiber-hydrogel composite were examined. Finally, using this nanofiber-hydrogel composite, a cartilage analog was developed to provide an off-the-shelf high-performance graft for tracheal cartilage regeneration, biomimetic artificial tracheal graft construction, and tracheal defect repair.

2. Materials and methods

2.1. Fabrication of OBC nanofibers and TGF-β modified fragmented OBC nanofibers

BC was produced by incubating Komagataeibacter xylinus X-2 in static culture for 7 days. 2,2,6,6-Tetramethylpyperidin-1-oxyl (TEMPO) oxidized BC nanofibers were prepared as previously described [19]. Briefly, BC pellicles (5 g) were added to deionized water (200 mL) containing TEMPO (0.05 g) and NaBr (0.5 g) and stirred at room temperature. Next, a 10 % NaClO solution was slowly added to initiate oxidation, with the reaction pH maintained at 10.5 by adding NaOH solution (0.5 M). Oxidation was quenched by adding 5 mL of absolute ethanol. The OBC nanofibers were rinsed with deionized water and lyophilized at −50 °C for 36 h.

OBC nanofibers (0.1 g) were cut into small pieces and subjected to mechanical defibrillation in deionized water (20 mL) using a high-speed homogenizer (FJ200-SH; Shuaijia Electron Sci. and Tech. Co., Ltd., Shanghai, China) at 13,000 rpm for 30 min to obtain fragmented short-length OBC (sOBC) nanofibers. The TGF-β solution was prepared by dissolving 50 μg of TGF-β in the 5 mL of 2-(n-morpholino)ethanesulfonic acid (MES) buffer. Subsequently, sOBC nanofibers (0.015g) were immersed in the TGF-β solution for 24 h at 25 °C. The obtained TGF-β modified sOBC (sOBC@TGF-β) nanofibers were washed with deionized water and stored at 4 °C.

2.2. Preparation of nanofiber-reinforced hydrogel composite

GelMA was dissolved in phosphate-buffered saline (PBS) (pH = 7.2–7.4) to prepare a 10 wt% precursor solution. The photo-initiator lithium phenyl-2,4,6-trimethyl-benzoyl phosphonate (LAP) with a concentration of 0.25 % was added to the solution. After agitation, homogeneous sOBC nanofibers with a concentration of 0.1 % were added and stirred for 2 h in the dark. The suspension solution was transferred into a mold with 365 nm ultraviolet (UV) light irradiation for 30 s. Four different hydrogel groups were established. The BG group represented GelMA hydrogel with sOBC nanofibers. In the case of BGF group, FGF at a concentration of 10 ng/mL was directly added to the sOBC nanofibers

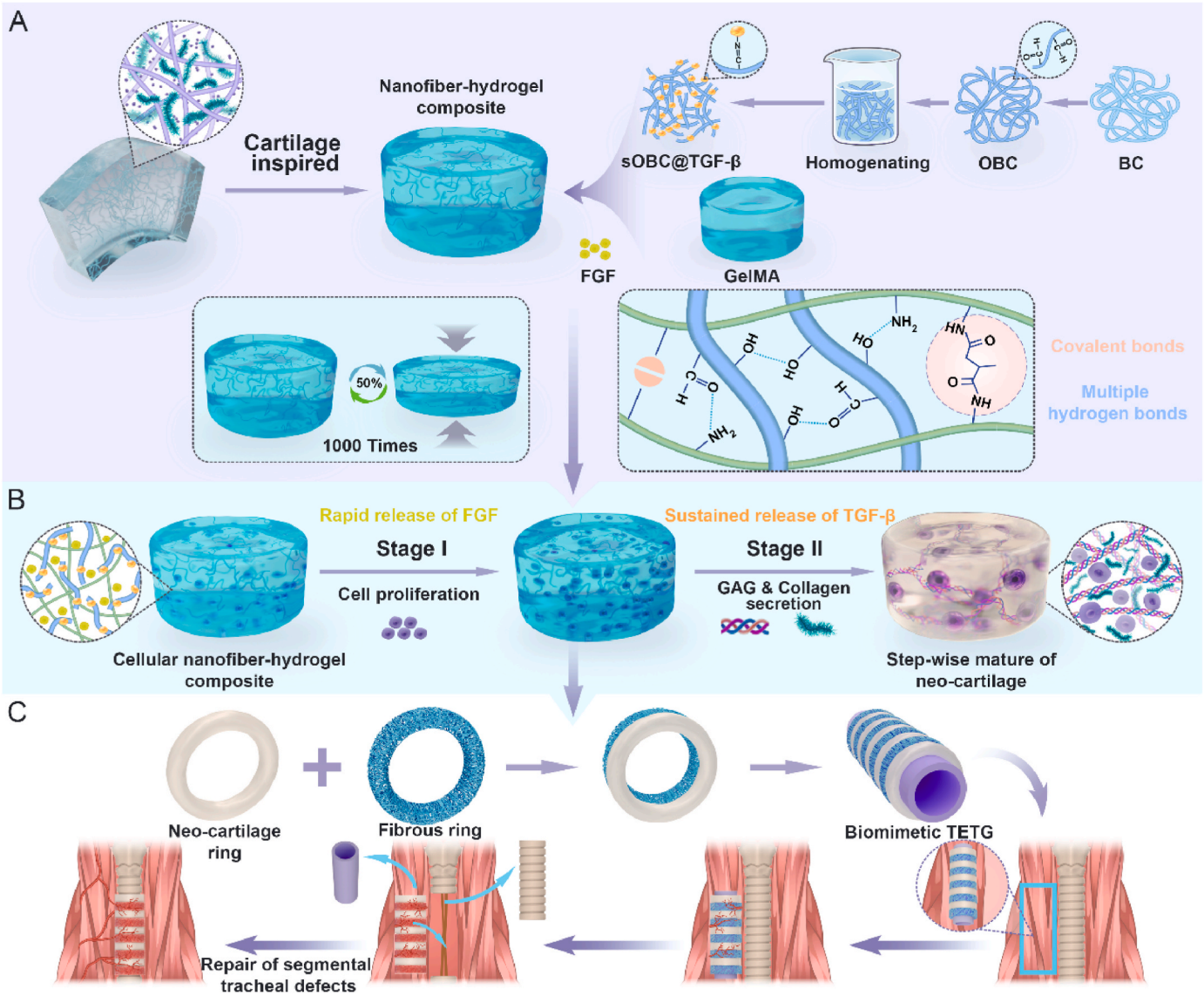

Scheme 1. Overview of the study. Schematic illustrating the neo-cartilage regeneration and biomimetic artificial tracheal grafts construction by the nanofiber-hydrogel composite. (A) The construction of nanofiber-hydrogel composite with superior mechanical performance and dual-release functionality of growth factors. (B) Representative biological events during the regeneration of neo-cartilage tissue by the nanofiber-hydrogel composite. (C) Construction of tissue-engineered biomimetic trachea and repair of segmental tracheal defects by the regenerated neo-cartilage tissue.

incorporated GelMA hydrogel before gelation. The BTG group represented GelMA hydrogel with sOBC@TGF-β nanofibers, whereas the BTGF group represented the nanofiber-hydrogel composite containing FGF and TGF-β growth factors.

2.3. Characterization of nanofibers and hydrogels

The samples of different hydrogels were prepared by freeze-drying at −40 °C for 48 h. Before the observation, the sections of the samples were cut and affixed to the electron microscope stage with conductive adhesive. The surface morphology of the material was examined using scanning electron microscopy (SEM, Nova Nano SEM 450, FEI Company, Oregon, USA) with an acceleration voltage of 10 kV following gold spraying for 30 s. The fiber diameter, length, and average pore size were measured using image analysis software (Nano Measurer 1.2, China). The chemical compositions of the samples were characterized using a Fourier transform infrared spectrometer (FTIR Spectrum II, PerkinElmer Inc., Massachusetts, USA). All spectra were obtained between 400 and 4000 cm^{-1} at a resolution of 4 cm^{-1}. The crystalline structure was characterized by X-ray diffraction (XRD, D8 ADVANCE, Bruker-Tech Co., Ltd., Karlsruhe, Germany).

2.3.1. Rheological testing of hydrogels and nanofiber-hydrogel composite

Rheological testing was performed to analyze the photosensitive properties of the nanofiber-reinforced hydrogel composite, following to a previous study [20]. The *in situ* photorheology was performed using a rotational rheometer (HAAKE MARS 360) at an angular frequency of 5 rad s^{-1} and 1 % strain to test the photosensitive properties of the hydrogel. The hydrogel samples were loaded at 37 °C for 18 s, followed by 20 s of UV light irradiation. After irradiation ceased, measurements continued for another 22 s. The storage modulus (G′) and loss modulus (G″) of the hydrogel samples were measured at a frequency of 1 Hz.

2.3.2. Swelling performance of hydrogels and nanofiber-hydrogel composite

To measure the swelling rate of samples, pregel solutions (500 μL) were injected into cylindrical molds and polymerized under UV light for 30 s. The samples were dried and weighed (recorded as W_0). The samples were then immersed in 5 mL of PBS (pH = 7.2–7.4) at 37 °C until

equilibrium was reached, and their weight changes were measured at different time points (recorded as W_1). The swelling rate was calculated as follows:

Swelling rate (%) = $([W_1\text{-}W_0])/W_0 \times 100\%$.

2.3.3. Water retention of hydrogels and nanofiber-hydrogel composite

The initial weight of the samples was recorded as W_0. The samples were then left in the air at 37 °C, and their weight (Wt) was measured at different time points. The water retention rate at time t was calculated using the following equation:

Water retention rate (%) = $([W_0\text{-}Wt]/W_0) \times 100\%$.

2.3.4. Analysis of mechanical properties

To evaluate the mechanical properties, the samples were molded into cylinders with a diameter of 10 mm and a height of 12 mm. The compressive properties of the samples were tested using a compression testing machine with a 100 N loaded sensor (MUF-1050, Tianjin Care Measure and Control Co., Ltd., Tianjin, China) at a compression rate of 5 mm/min. Repeated compression tests, as an anti-fatigue assay, were performed 1000 times at a strain ratio of 50 %.

2.4. Release profiles of FGF and TGF-β

The nanofiber-hydrogel composites were placed in test tubes containing 1 ml of PBS. The tubes were incubated in a shaking bath at 30 rpm and 37 °C. At each time point, the supernatants were collected and replaced with an equal volume of fresh PBS. The concentrations of FGF and TGF-β were measured using an enzyme-linked immunosorbent assay (ELISA) kit, according to the manufacturer's instructions.

2.5. Isolation and culture of chondrocytes

Rabbit auricular chondrocytes were isolated as previously described [16,21]. Briefly, auricular cartilage was minced into 1×1 mm^2 pieces and digested using 0.15 wt% collagenase Type II to obtain chondrocytes. Harvested chondrocytes were cultured and expanded in Dulbecco's modified Eagle's medium (DMEM, Gibco) supplemented with 10 % fetal bovine serum (FBS, Gibco) and 1 % penicillin−streptomycin. Chondrocytes in passage two were used for the following studies.

2.6. Biocompatibility of nanofiber-hydrogel composite

The chondrocytes at a density of 1×10^6 cells/mL were encapsulated in different nanofiber-hydrogel composites. After culturing for 1, 5, and 10 days *in vitro*, the chondrocyte-hydrogel constructs were removed and washed with PBS solution. Then, the Live & Dead staining was performed according to the manufacturer's instructions. Chondrocyte proliferation within the hydrogel was evaluated using the Cell Counting Kit-8 (CCK-8) assay on days 1, 5, and 10. The optical density at 450 nm (OD450) was measured using an automated plate reader.

2.7. Engineering of cell-hydrogel constructs and evaluation of neo-cartilage cultured in vitro and in vivo

The chondrocytes were encapsulated in different nanofiber-hydrogel composites. The cell seeding density for the BGF, BTG, and BTGF hydrogels was 20 million cells/mL. For the BG hydrogel, cell densities of 20 and 40 million cells/mL were utilized. After hydrogel gelation, the cell-hydrogel construct (6 mm diameter and 2 mm height) was gently transferred into and submerged in the culture medium. After culturing for 5 days, the cell-hydrogel constructs were then cultured in a chondrogenic medium as previously described and harvested after 1 and 4 weeks of *in vitro* culture [22,23]. For *in vivo* cartilage regeneration evaluation, the constructs were subcutaneously implanted into the dorsal flanks of nude mice (4–6 weeks old). After 1 and 4 weeks of implantation, the samples were harvested to evaluate cartilage regeneration. Tissue constructs for trachea-shaped, ring-like cartilage (10 mm external diameter, 6 mm internal diameter, and 1.5 mm height) were prepared. *In vitro* and *in vivo* cartilage regeneration were performed.

2.8. Histological, biochemical and biomechanical evaluation of regenerated cartilage tissue

The harvested constructs were fixed in a 4 % paraformaldehyde solution for 24 h, dehydrated, embedded in paraffin, and sectioned at 4 μm. Sections were stained with hematoxylin and eosin (HE) to identify tissue morphology. Safranin-O staining was performed to assess the production of proteoglycans within the matrix, whereas Masson's trichrome (MT) staining was used to detect collagen deposition. Type I and II collagen staining was performed to evaluate extracellular collagen deposition of neo-cartilage tissue. Stained sections were analyzed under a microscope. The Bern score was used to evaluate *in vitro*-engineered cartilaginous tissues [24].

The harvested samples were minced to conduct cartilage-related biochemical evaluations for glycosaminoglycans (GAG) and total collagen, which were quantified using the dimethylmethylene blue and hydroxyproline assay kits (Nanjing Jiancheng Bioengineering, China) according to the manufacturer's protocols. The mechanical properties were measured using a mechanical analyzer, and the slope of the linear stress–strain curve was defined as the compressive modulus [4].

2.9. Regeneration of tissue-engineered trachea in vivo

A tissue-engineered trachea graft was prepared using trachea-shaped, ring-like cartilage and a BC macroporous scaffold. The cartilage and BC rings were stacked alternately on a silicon tube. The tissue-engineered trachea was subcutaneously implanted into the dorsal flanks of nude mice (4–6 weeks old). After 4 weeks of implantation, the samples were harvested for evaluation of cartilage regeneration.

2.10. Tissue-engineered tracheal graft transplantation in rabbits

All animal care, housing conditions, and experimental protocols were strictly in compliance with the Guide for the Care and Use of Laboratory Animals of the Shanghai Pulmonary Hospital Ethics Committee, ensuring ethical treatment of the animals and scientific rigor in our study. The 6 to 8-week-old New Zealand rabbits were used in our study. The rabbits were anesthetized with an intramuscular injection of ketamine (5 mg/kg) and inhaled isoflurane. A midline incision was made in the anterior neck and the strap muscles were carefully separated to create a pocket. A tissue-engineered trachea graft, supported by a silicone tube, was subsequently placed into the pocket. Finally, the intramuscular pocket and skin incisions were closed. Repair and reconstruction of segmental tracheal defects were performed 4 weeks after intermuscular implantation of a biomimetic tissue-engineered tracheal graft. A median cervical incision was made to expose the trachea. The encapsulated tissue-engineered trachea graft was gently dissociated from the surrounding tissue to form an integrated segmental tracheal organoid unit. During this procedure, the blood supply to the trachea grafts had to be preserved. After the removal of the supporting silicone tube, both ends of the engineered trachea were trimmed. A segment of the native trachea with a length similar to that of the artificial trachea was removed. The tissue-engineered trachea was implanted, and an end-to-end continuous anastomosis was circumferentially performed to restore the integrity of the trachea. The incisions were then closed in layers. The animals were sacrificed at designated time points, and the reconstructed trachea was observed grossly and histologically.

2.11. Statistical analysis

Continuous variables were expressed as mean ± standard deviation (SD). Statistical analyses were performed using SPSS software (version17.0) and Graphpad Prism 8.0 software. For statistical analysis, one-way ANOVA was performed, followed by Tukey's post-hoc test, and statistical significance was indicated by p-values: $*p < 0.05$, $**p < 0.01$.

3. Results

3.1. Preparation and characterization of TGF-β modified sOBC nanofibers

The preparation process of TGF-β modified fragmented sOBC nanofibers is shown in Fig. 1A. The diameter of the OBC nanofibers was significantly reduced after TEMPO oxidation compared to that of the BC nanofibers (Fig. 1B and C, Fig. S1A and B). The OBC nanofibers were mechanically homogenized into fragmented sOBC nanofibers to achieve more uniform biomolecule loading and distribution within the hydrogel solution (Fig. 1D and S1C). Furthermore, TGF-β was loaded on the surface of sOBC via a Schiff-base reaction. The chemical characteristics of different samples were investigated using FTIR spectroscopy (Fig. 1E). The absorption peaks at 3347, 2896, and 1058 cm^{-1} corresponded to the contraction vibration of the OH group, the stretching vibration peak of the C–H bond, and the vibration peak of C–O–C of BC, respectively. For the spectra of OBC, the characteristic peak of carbonyl groups appeared at 1730 cm^{-1}, indicating that the BC had been oxidized. The absorption at 1656 cm^{-1}, resulting from the imine band (C=N), verified the formation of the condensation reaction between TGF-β and sOBC, confirming the Schiff-base formation.

The XRD patterns of the samples are shown in Fig. 1F. Three peaks at 14.1°, 16.5°, and 22.4° can be observed in all the patterns, corresponding to the (110), (1_10), and (200) crystal planes of cellulose I crystals. Furthermore, the three diffraction peaks of BC become more wider and weaker after TEMPO oxidation and TGF-β loading, which indicated the reduction of crystallinity. In addition, fluorescence-labeled TGF-β loaded on the sOBC nanofiber was visualized using confocal laser scanning microscopy (CLSM), suggesting that TGF-β was successfully loaded and uniformly distributed on the surface of sOBC (Fig. 1G). Therefore, an effective nanocarriers were developed for the loading and delivery of functional biomolecules.

3.2. Preparation and characterization of nanofiber-hydrogel composite

To mimic the natural cartilage ECM structure, the homogenized sOBC@TGF-β nanofiber was introduced into GelMA hydrogel to obtain a mechanically reinforced biomimetic hydrogel. FTIR results demonstrated the successful combination of sOBC@TGF-β nanofiber and GelMA (Fig. 2A). Rheological tests were conducted to evaluate the photosensitivity of the hydrogel, showing that the sol-to-gel transition of the mechanically reinforced biomimetic hydrogel upon UV light irradiation was unchanged compared with that of the GelMA hydrogel (Fig. 2B and C). The results indicated that the BTG hydrogel could rapidly crosslink within a short and safe exposure time. The hydrogel was further molded into tracheal cartilage rings after UV irradiation (Fig. 2D). SEM images showed that the nanofibers were uniformly dispersed within the pore walls, and the resulting nanofiber-hydrogel composite exhibited a denser structure than the GelMA hydrogel (Fig. 2E). The pore size of the BTG hydrogel was smaller than that of the GelMA hydrogel (Fig. 2F, Fig. S2A and B). The BTG hydrogel exhibited a lower swelling ratio and higher water retention rate owing to the introduction of the sOBC nanofibers (Fig. 2G and H). An evenly distributed green fluorescence signal was detected within the BTG hydrogel, suggesting that the TGF-β modified sOBC nanofibers achieved uniform distribution within the GelMA hydrogel (Fig. S2C).

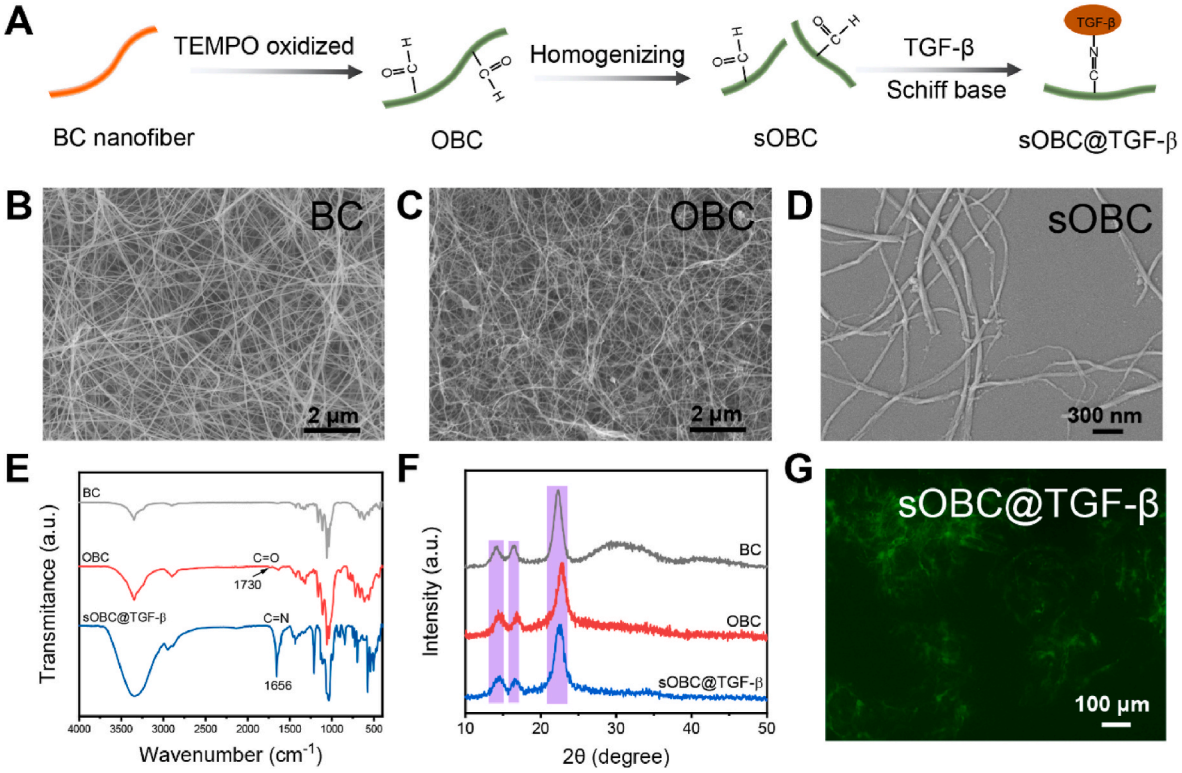

Fig. 1. Preparation and characterization of TGF-β modified sOBC nanofibers. (A) Schematic diagram of the preparation of the TGF-β modified sOBC nanofibers. (B–D) SEM images of the BC, OBC, and homogenized sOBC nanofibers. (E) FTIR spectra of BC, OBC, and sOBC@TGF-β nanofibers. (F) XRD patterns of BC, OBC, and sOBC@TGF-β nanofibers. (G) CLSM images of TGF-β loaded sOBC nanofibers.

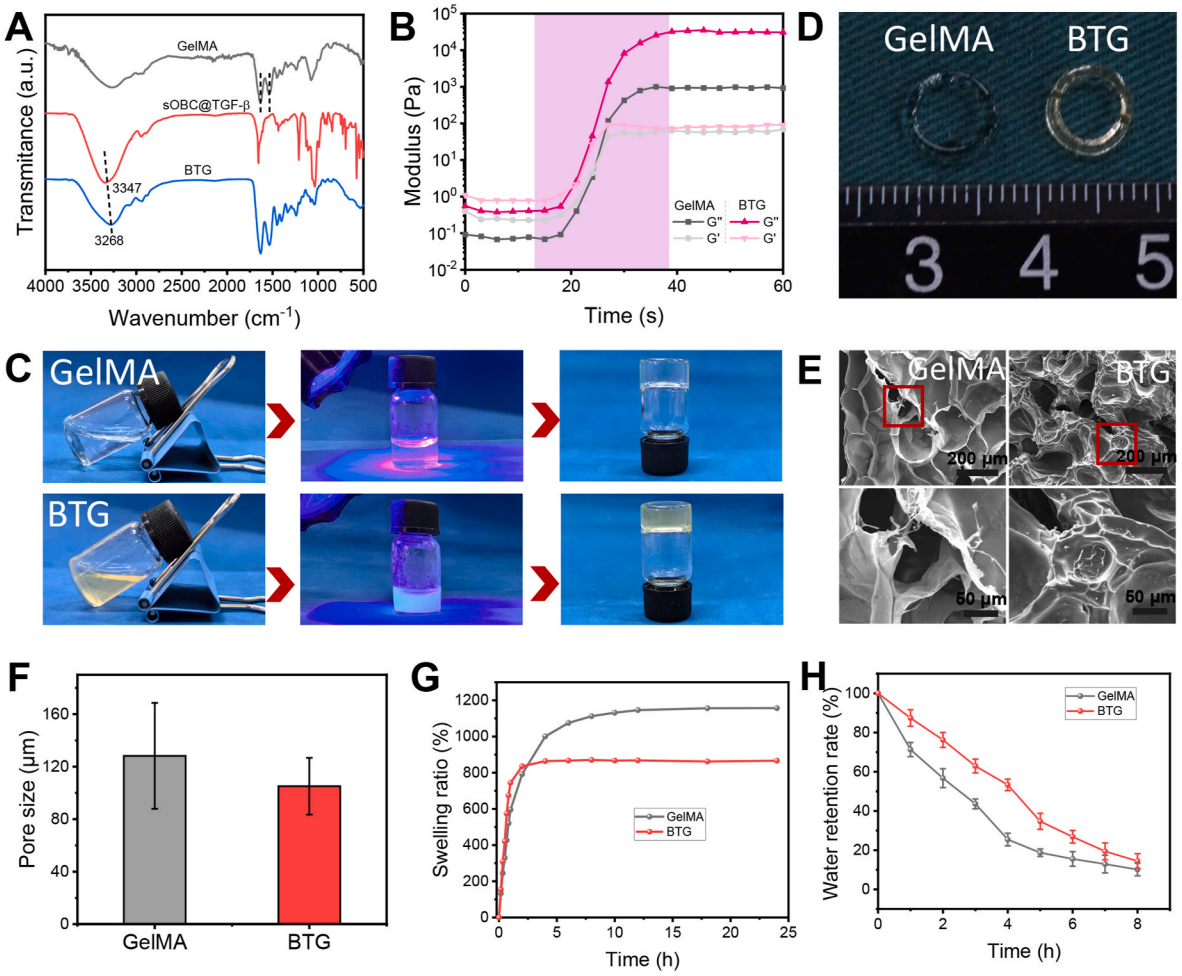

Fig. 2. Characterization of GelMA hydrogel and nanofiber-hydrogel composite. (A) FTIR spectra of GelMA, sOBC@TGF-β nanofibers, and BTG hydrogel. (B) Photosensitivity of GelMA and BTG hydrogel. (C) Digital photographs of the sol-to-gel transition upon UV light irradiation. (D) Digital photographs of the ring-shaped hydrogel. (E) SEM images of GelMA and BTG hydrogel. (F) Pore size distribution of GelMA and BTG hydrogel. (G and H) Swelling ratio and water retention rate of GelMA and BTG hydrogel.

3.3. Mechanical performance of nanofiber-hydrogel composite

The introduction of sOBC@TGF-β nanofiber not only constructed the biomimetic cartilage ECM but also significantly enhanced the elastic mechanical behavior of the GelMA hydrogel. The compressive stress–strain profiles of the hydrogel were tested to investigate the effect of the nanofibers on its mechanical properties (Fig. 3A). The mechanically reinforced hydrogels exhibited higher stress and strain values than the GelMA hydrogel. The GelMA hydrogel underwent severe mechanical damage at 70 % strain, whereas the BTG hydrogel withstood higher compressive stress and maintained its integrity at 85 % strain. Furthermore, the BTG hydrogel exhibited excellent mechanical resilience and recovered its original shape without any obvious deformation under compression (Fig. 3B). After three stepped compression cycles at 40, 60, and 80 % strains, the BTG hydrogel maintained its original state (Fig. 3C). The maximum stress of the GelMA hydrogel decreased by more than 15 %, and obvious cracks appeared on the cylinder after 100 compression-release cycles at 50 % strain (Fig. 3D). Notably, the BTG hydrogel recovered its original shape without obvious plastic deformation or structural damage after 100 cycles, indicating excellent structural stability (Fig. 3E). More importantly, the fatigue performance of the BTG hydrogels was evaluated. Fig. 3F indicates that only a 4.5 % reduction in compressive stress was observed at 50 % strain after 1000 cycles. This superb stability can be explained by Fig. 3G, which shows that the introduction of sOBC@TGF-β nanofibers further enhances the crosslinking effect of GelMA molecular chains. These stress-retention behaviors are superior in meeting the requirements for tracheal cartilage regeneration.

3.4. Evaluation of chondrocyte viability and proliferation in hydrogels

Based on the nanofiber-hydrogel composite, a dual growth factor release system was designed to promote cell proliferation and achieve optimal differentiation of encapsulated chondrocytes through sequential growth factor release (Fig. 4A). FGF was embedded within the GelMA hydrogel, followed by incorporation of TGF-β modified sOBC nanofibers. The release profiles of FGF and TGF-β from the nanofiber-hydrogel composite are shown in Fig. S3. A relatively faster release of FGF, along with a sustained and slower release of TGF-β, was observed. Within 24 h, approximately 60 % of FGF stored in the GelMA hydrogel was released, whereas the cumulative release percentage of TGF-β was approximately 3 %. By the end of the measurement period, the release percentage for TGF-β reached approximately 49 %. Hence, a novel bioengineering system was developed to achieve differentiated release profiles of FGF and TGF-β for inducing a synergistic effect on cartilage regeneration.

Then, the above hydrogel was used as a chondrocyte carrier to form cell-hydrogel constructs. Cell viability and proliferation were evaluated using Live & Dead staining. A BG hydrogel without growth factors was used as the control group. The CLSM images showed that visible

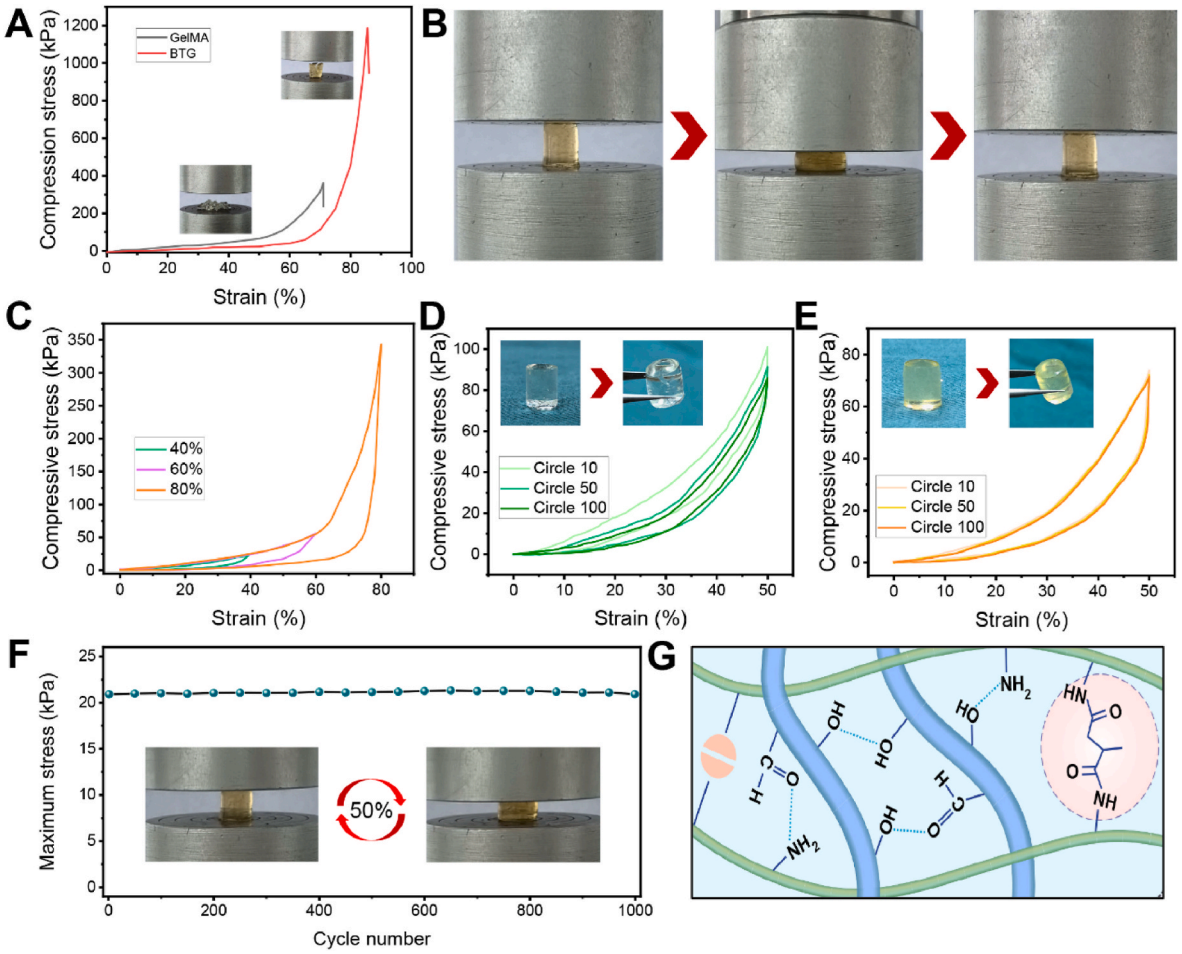

Fig. 3. Mechanical properties of the nanofiber-hydrogel composite. (A) Stress–strain curve of GelMA and BTG hydrogel. (B) Digital photographs of the BTG hydrogel during compression and recovery process. (C) Stress–strain curve of BTG hydrogel under different strains (40, 60, and 80 %). (D and E) 100 times of compressive loading–unloading cycle for GelMA and BTG hydrogel. (F) Mechanical performance of BTG hydrogel after 1000 times of compressive loading–unloading cycle. (G) Schematic illustration of mechanically reinforced biomimetic hydrogel.

fluorescence intensity continuously increased with longer culture time and almost no dead cells were detected, indicating that the hydrogel exhibited good biocompatibility (Fig. 4B and Fig. S4). The BTGF hydrogel group exhibited the highest recorded integrated density of green fluorescence after 10 days of culture, indicating a significant increase in cell number (Fig. 4C). In addition to the qualitative evaluation, chondrocyte proliferation was quantitatively assessed using the CCK-8 assay. The cell population significantly increased with prolonged culture from 1 to 10 days (Fig. 4D). For the BGF hydrogel, cell numbers significantly increased after 5 days, and a similar growth trend was noted in the presence of TGF-β, though to a lesser extent. Notably, the chondrocytes displayed a significantly higher proliferation rate in the BTGF group than in the BTG and BGF groups, indicating the high proliferative potential of the cells in the dual growth factor-laden hydrogel.

3.5. *Evaluation of cartilage regeneration by nanofiber-hydrogel composite in vitro*

We conducted an in-depth assessment to determine the potential of the nanofiber-hydrogel composite for neo-cartilage regeneration through *in vitro* chondrocyte encapsulation. Chondrocyte seeding densities of 20 million (BG-20M, BGF-20M, BTG-20M, and BTGF-20M) and 40 million (BG-40M) cells/mL were used to evaluate the efficiency of the optimal bioengineered hydrogel system to obtain functionally transplantable cartilage analogs. After 1 week of cultivation, HE staining results showed that chondrocytes in the growth factor-loaded hydrogel exhibited significantly higher expression of cartilage ECM than those in the control group (Fig. 5A). A similar trend was observed in safranin-O staining for GAG, reflecting the levels of cartilage-specific proteoglycans and ECM. Compared to the FGF-laden hydrogel, the TGF-β laden hydrogel showed partial cartilage with strong positive staining for safranin-O. Furthermore, even with considerable GAG deposition in the BTGF-20M group, the staining density was relatively lower than that in the BG-40M group. Immunohistochemical staining showed that the deposition of type II collagen was higher in the BTGF-20M and BG-40M hydrogel groups than in the other groups.

After 4 weeks of *in vitro* cultivation, histological analysis revealed that the morphologies of the partial chondrocytes within the hydrogel were typical of chondrocytes (Fig. 5B). Safranin-O and collagen staining qualitatively reflected time-dependent trends in cartilage-specific matrix deposition. Constructs with sole stimulation of FGF or TGF-β produced significantly more GAG content compared to BG-20M hydrogel. The sole exposure of chondrocytes to FGF in the BGF-20M hydrogel did not significantly affect GAG production, compared with the BTG-20M hydrogel group. Compared with those in the BTG-20M and BGF-20M groups, more homogenous cartilage-specific ECM deposition and chondral tissue maturation were observed in the BTGF-20M and BG-40M groups. Furthermore, the collagen immunohistochemical staining results were consistent with those of GAG, displaying enhanced type II collagen content when exposed to dual growth factor stimulation and high cell seeding density. Regenerated neo-cartilage *in vitro* in all hydrogel group showed a limited expression of type I collagen in the

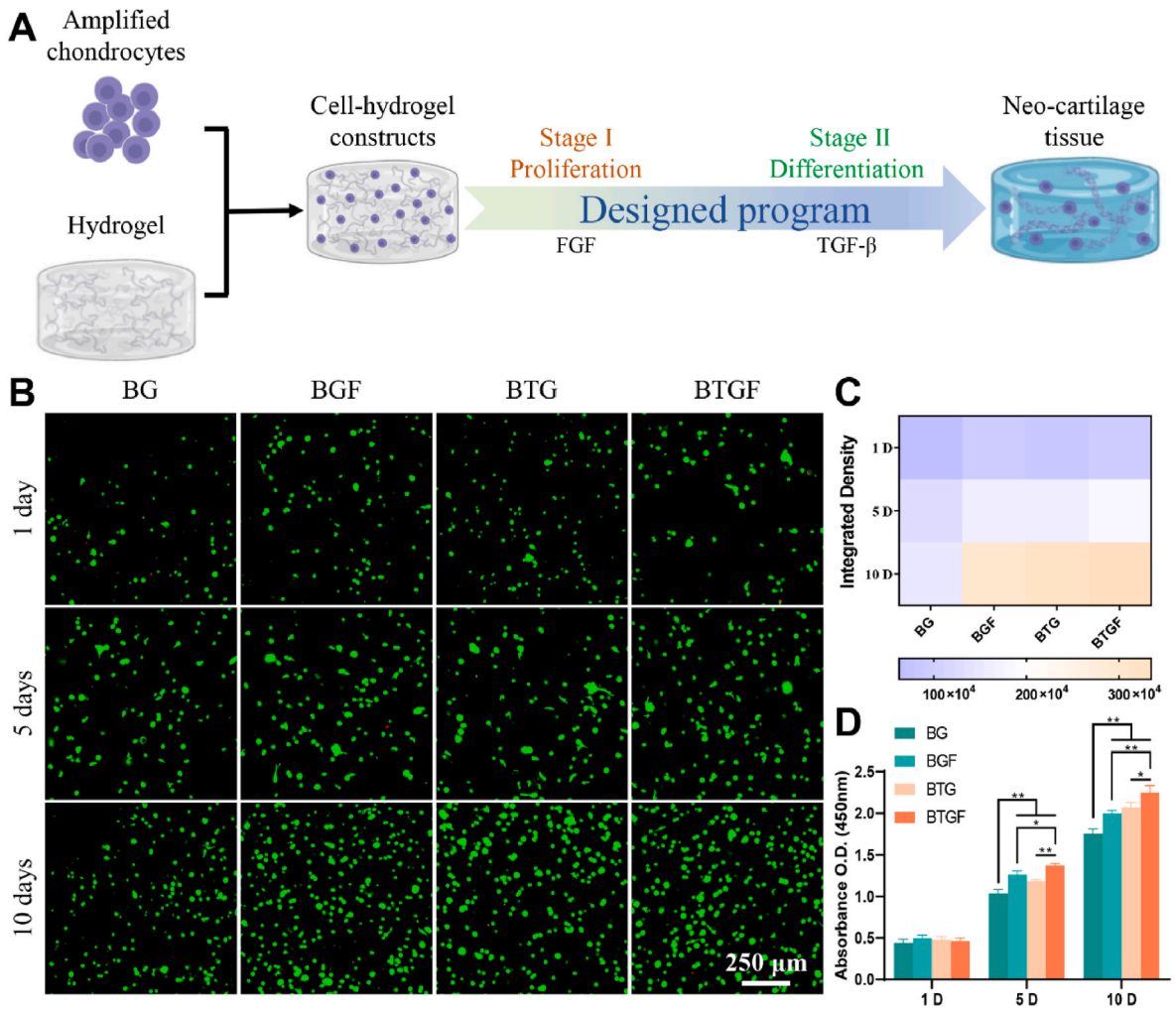

Fig. 4. Cell viability and proliferation assay for chondrocytes in hydrogel. (A) Schematic diagram illustrating the designed program for the formation of mature neo-cartilage tissue. (B) Confocal microscopic images for Live and Dead staining (live cells, green fluorescence; dead cells, red fluorescence). (C) Integrated density of green fluorescence (live chondrocytes) at various culture times. (D) CCK-8 assay for cell proliferation rate after different culture periods (n = 3 independent samples, *: $p < 0.05$, **$p < 0.01$).

neo-cartilage body (Fig. S5). Therefore, it can be deduced that the synergistic effect of growth factors on cell proliferation and chondrogenesis results in better cartilage regeneration with abundant ECM deposition. The Bern score was used to evaluate the quality of *in vitro* engineered cartilaginous tissue (Fig. 5C). The results showed that the BTGF-20M group achieved uniform and intensive matrix deposition, appropriate cell density with an extensive matrix, and a rounded chondrocyte morphology comparable to that of the BG-40M group. Consistent with the histological results, quantitative analyses further revealed that the engineered cartilage tissue in the BTGF-20M group exhibited higher DNA, GAG, and collagen contents than the BG-20M, BTG-20M, and BGF-20M groups (Fig. 5D). Although the collagen content in the BTGF-20M group was lower than that in the BG-40M group, there was no significant difference in the DNA and GAG content between the BTGF-20M and BG-40M groups.

3.6. *Evaluation of cartilage regeneration by nanofiber-hydrogel composite in vivo*

Subcutaneous implantation was performed in nude mice to evaluate cartilage regeneration *in vivo* (Fig. 6A). Almost no obvious cartilage tissue was observed in the BG-20M group 1 week after subcutaneous implantation (Fig. 6B). In contrast, the addition of FGF or TGF-β growth factor within the hydrogel produced more cell populations with enriched ECM, although no significant safranin-O and type II collagen staining was observed. The constructs in the BTGF-20M group showed scattered cartilage islands with positive staining for cartilage-specific ECM, whereas tissues in the BG-40M group showed relatively broad regions exhibiting cartilage-specific ECM formation.

Four weeks after implantation, a typical lacunae structure was observed in the neo-cartilage tissue formed by different hydrogels (Fig. S6). The BG-20M group showed dense fibrillar tissue invasion and minimal cartilage-specific matrix production, whereas the other four groups exhibited robust newly synthesized cartilage matrix that was positive for safranin-O and type II collagen, indicating stronger chondroinductive capabilities (Fig. 6C and Fig. S7). However, the matrix deposition was nonuniform in the BGF-20M and BTG-20M groups. In contrast, the BTGF-20M and BG-40M groups exhibited uniform matrix deposition. Immunohistochemical staining revealed more intense type II collagen staining in the BTGF-20M and BG-40M groups hydrogel compared to the BG-20M, BGF-20M, and BTG-20M groups. Furthermore, quantitative and mechanical analysis showed no significant difference in cartilage-specific ECM deposition and biomechanical performance between the BTGF-20M and BG-40M groups after *in vivo* culture, indicating that the dual growth factor-laden nanofiber-hydrogel group effectively formed robust neo-cartilage tissue with homogeneous ECM, similar to the high cell seeding density group (Fig. S8).

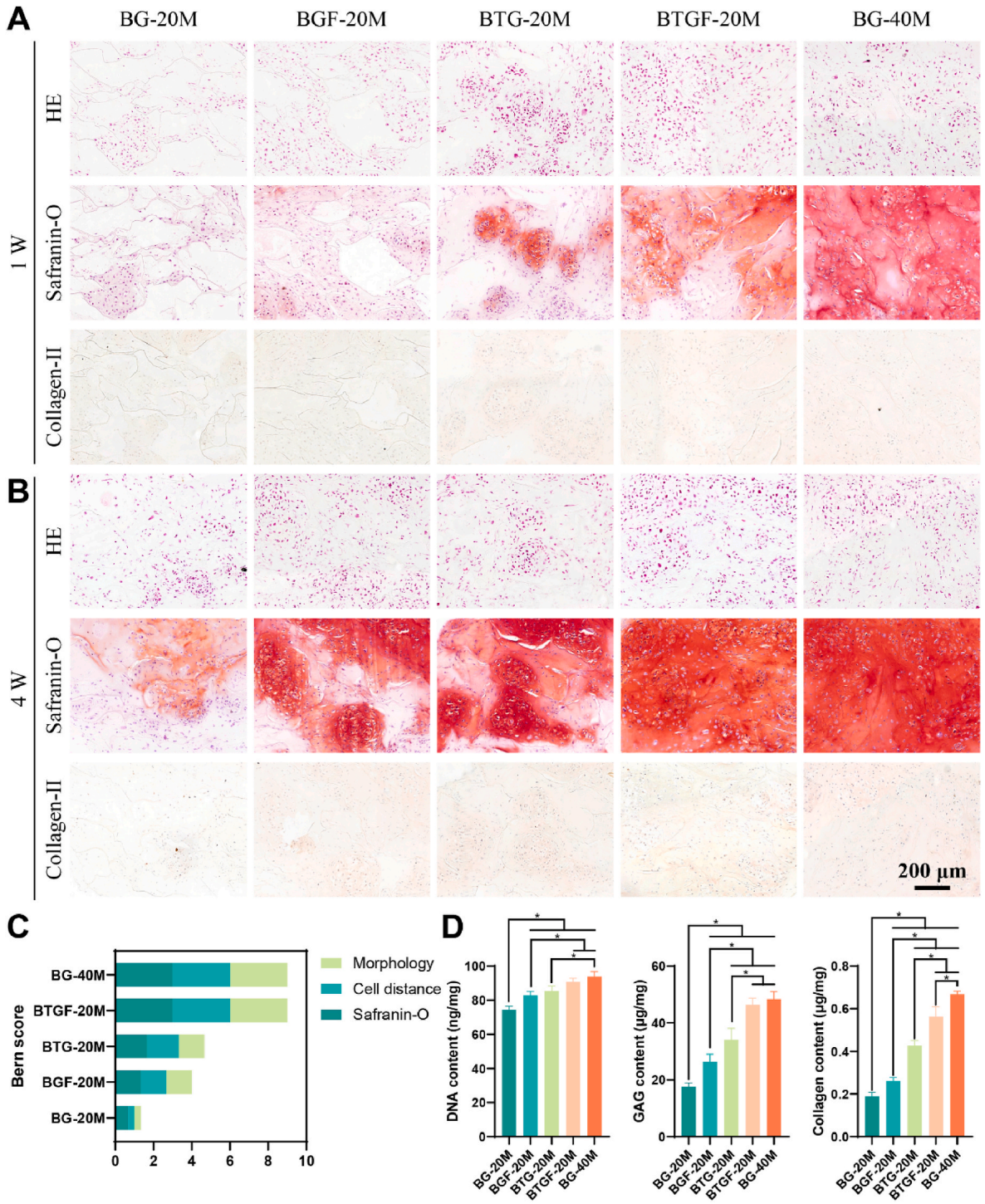

Fig. 5. Histological analysis of chondrocyte-laden hydrogel for cartilage tissue regeneration *in vitro*. (A) Representative HE, safranin-O, and type II collagen staining of constructs after 1 week *in vitro* culture. (B) Representative HE, safranin-O, and type II collagen staining of constructs after 4 weeks *in vitro* culture. (C) The Bern score for the regenerated neo-cartilage tissue after 4 weeks of *in vitro* culture. (D) Quantitative evaluation of DNA content, GAG content, and collagen content in neo-cartilage tissue after 4 weeks of *in vitro* culture (n = 3 independent samples, *: $p < 0.05$).

3.7. Regeneration of trachea-shaped ring-like cartilage in vitro and in vivo

Although the above results confirm the feasibility of constructing biochemically and biomechanically robust mature cartilage with BTGF-20M, further research is needed to develop ring-shaped tracheal cartilage tissue with a stable geometric shape, high fidelity, and superior mechanical performance. We assessed the efficacy of the cell-laden hydrogel (BTGF-20M) for ring-shaped cartilage regeneration. The cell-laden constructs formed preliminary cartilage-like tissue after 4 weeks of *in vitro* culture, with histological staining showing abundant cartilage-specific ECM deposition (Fig. 7A). Furthermore, mature cartilage with a white and smooth appearance was obtained after *in vivo* subcutaneous implantation (Fig. 7B). Histological results demonstrated abundant cartilage-specific ECM deposition, with strong positive staining for safranin-O and type II collagen. Morphological changes were observed in the inner diameter of the cartilage rings. The cartilage rings

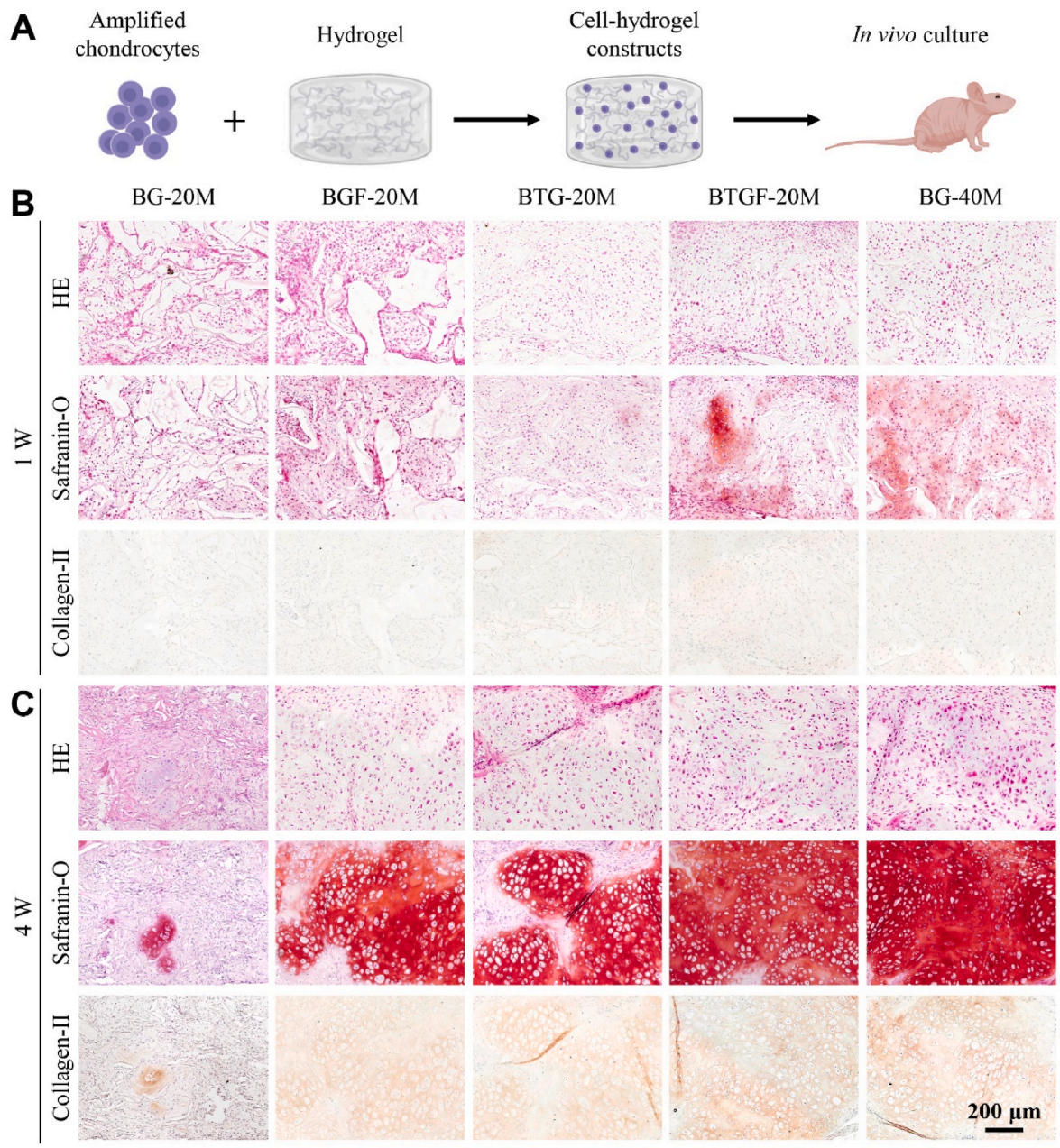

Fig. 6. Histological evaluation of chondrocyte-laden hydrogel for cartilage tissue engineering in the dorsal subcutaneous area of nude mice. (A) Schematic diagram illustrating the fabrication of chondrocyte-laden hydrogel for *in vivo* cartilage regeneration. (B) Representative HE, safranin-O, and type II collagen staining of the chondrocyte-hydrogel constructs after 1 week *in vivo* culture. (C) Representative HE, safranin-O, and type II collagen staining of the chondrocyte-hydrogel constructs after 4 weeks *in vivo* culture.

constructed *in vivo* shrank compared with those constructed *in vitro*, resulting in slight decrease in the inner diameter (Fig. 7C). Quantitative analysis demonstrated that cartilage rings *in vivo* present superior mechanical properties and higher contents of GAG and collagen compared to those *in vitro*.

3.8. Construction of tissue-engineered biomimetic trachea

To further investigate the feasibility of using cellular hydrogel to construct tracheal grafts, cartilage rings formed by the BTGF hydrogel were stacked with fibrous rings to prepare an artificial tissue-engineered trachea. The biomimetic tracheal grafts were subcutaneously implanted into nude mice with a silicone tube support to maintain their inner diameter. After 4 weeks of *in vivo* implantation, the alternating cartilage and fibrous rings were successfully fused into an artificial trachea with a tubular shape, featuring seamless junctions between the rings (Fig. 8A). The lumen of the tissue-engineered trachea was smooth and well-preserved in the lateral view. Histological examination confirmed the regeneration of the biomimetic tracheal structure and cartilage tissue (Fig. 8B). The cartilage ring in the tissue-engineered trachea exhibited a typical lacuna structure with cartilage-specific ECM deposition, similar to native tracheal cartilage (Fig. 8C and Fig. S9). Histological and immunohistological staining of the longitudinal section of the engineered trachea showed that the structure of cartilage rings was arranged at intervals, resembling the native rabbit trachea (Fig. 8D).

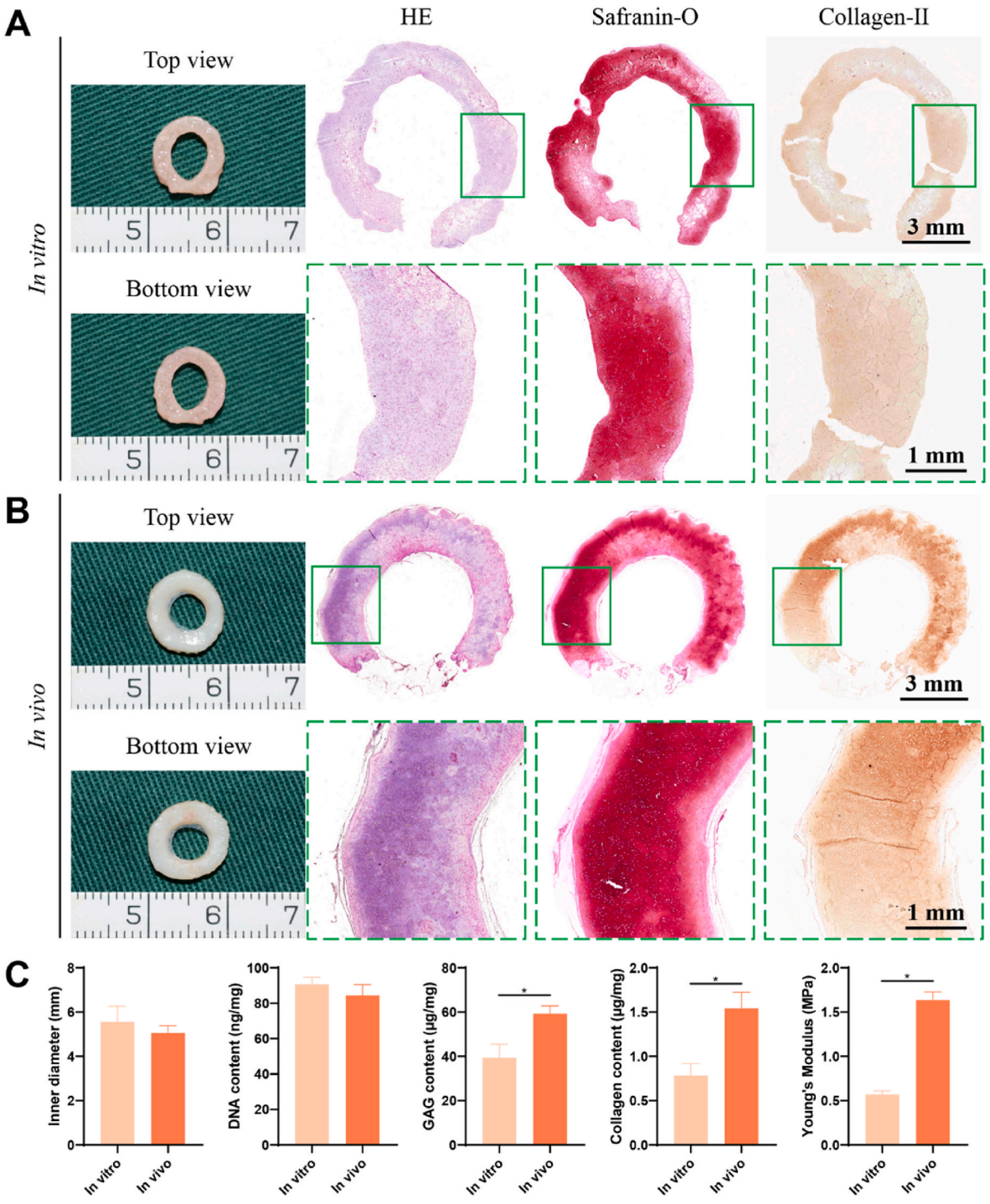

Fig. 7. Fabrication and characterization of trachea-shaped ring-like cartilage. (A) Gross images and histological staining (HE, safranin-O, and type II collagen) of trachea-shaped ring-like cartilage *in vitro*. (B) Gross images and histological staining (HE, safranin-O, and type II collagen) of trachea-shaped ring-like cartilage *in vivo*. (C) Quantitative analysis of inner diameter, Young's modulus, and the amounts of DNA, GAG, as well as collagen in the engineered cartilage *in vitro* and *in vivo* (n = 3 independent samples, *: $p < 0.05$).

3.9. Segmental reconstruction with tissue-engineered trachea in a rabbit model

We investigated the clinical applicability of tissue-engineered tracheal grafts for functional tracheal reconstruction. Four weeks after intramuscular implantation, the biomimetic trachea maintained its original shape and was surrounded by a well-vascularized muscle flap (Fig. S10 and Fig. 9A). A longitudinal view of the regenerated trachea is shown in Fig. 9A. After removing the silicone stent, the trachea substitutes maintained their cylindrical shape, with no collapse observed. Subsequently, a segment of the native trachea, similar in length to the tissue-engineered trachea grafts, was excised, and the trachea graft was implanted to restore tracheal integrity through end-to-end anastomosis.

Of the six experimental rabbits, a survival rate of 83.3 % was observed, with five rabbits surviving. One rabbit died because of post-operative airway obstruction (Fig. S11). An X-ray examination revealed that the luminal patency of the implanted tracheal grafts was

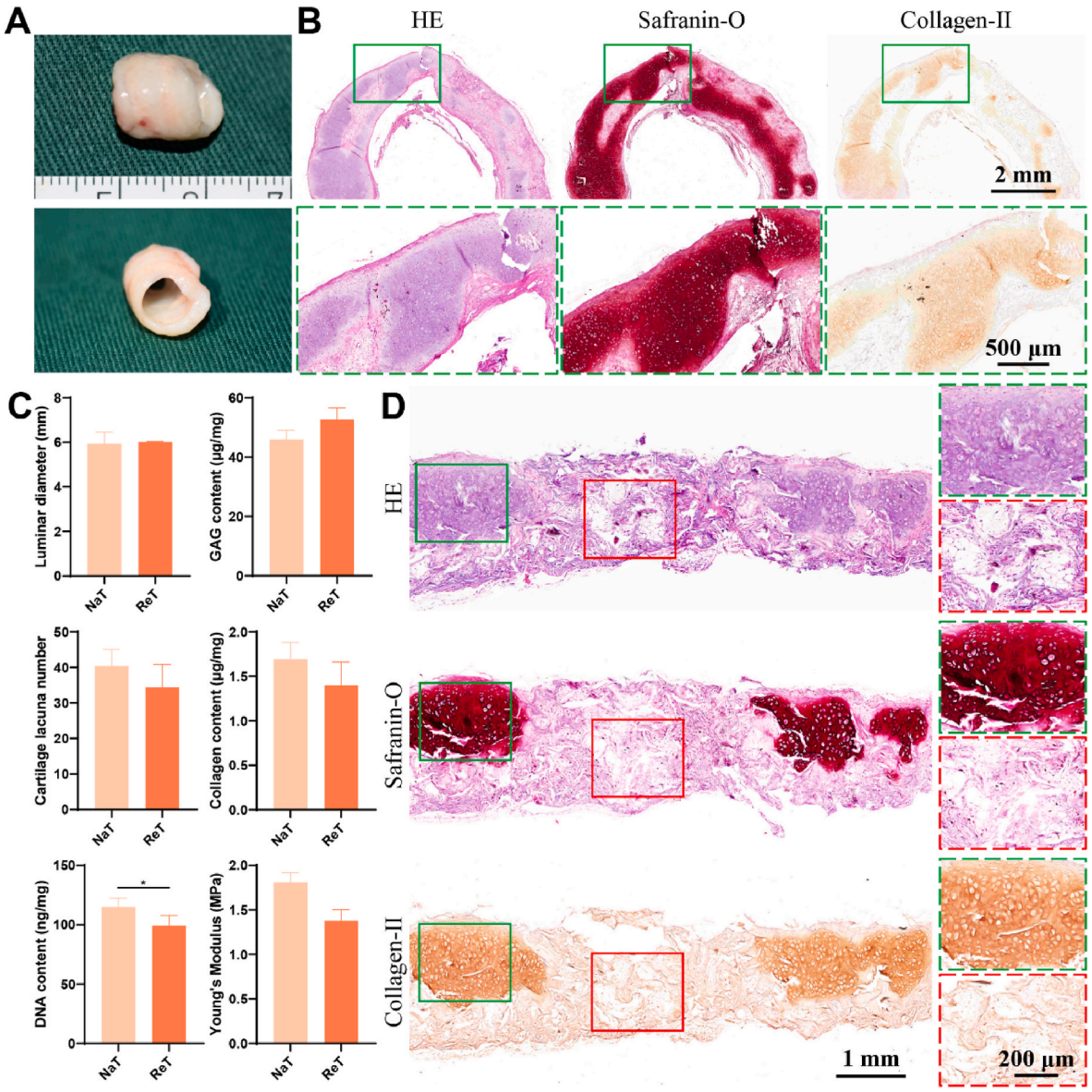

Fig. 8. Construction of tissue-engineered biomimetic trachea grafts. (A) Macroscopic images of trachea grafts after 4 weeks of subcutaneous implantation in nude mice *in vivo*. (B) Histological and immunohistological analysis of trachea grafts in the transverse sections. (C) Morphological and histological quantitative analysis of trachea grafts compared to native rabbit trachea cartilage (n = 3 independent samples, *: $p < 0.05$). (D) Histological and immunohistological analysis of tissue-engineered trachea grafts in longitudinal sections.

maintained 4 weeks after surgery (Fig. 9B). Bronchoscopic examination revealed that the inner surface of the engineered trachea was smooth (Fig. 9C). A continuous patent lumen of the reconstructed trachea was observed from the anastomotic site to the other side, with no obvious formation of hyperplastic granulation tissue or tracheal. Macroscopic images of the luminal areas of the retrieved implants indicated good integration with the native trachea (Fig. 9D). Histological staining of the neo-cartilage demonstrated cartilage-specific features, including lacunae structures, cartilage-specific ECM, and type II collagen deposition (Fig. 9E). Vascularized capsular tissue with numerous small blood vessels was observed outside the fibrous-ring compartment of the pedicled artificial trachea, indicating adequate vascularization of the reconstructed trachea (Fig. S12). Histological analysis of longitudinal sections of the reconstructed trachea indicated an alternating pattern of cartilaginous tissue and fibrous tissue, resembling the native trachea (Fig. 9F). Morphological analysis of the artificial tracheal neo-cartilage showed structural characteristics similar to those of native tracheal cartilage (Fig. 9G). These results demonstrate the feasibility of employing tissue-engineered trachea grafts from chondrocytes loaded BTGF hydrogel for functional tracheal reconstruction.

4. Discussion

Several tissue compartments constitute a functional tracheal organ, including the endoderm-derived pseudostratified columnar epithelium and mesoderm-derived mesenchyme, such as C-shaped cartilage rings and smooth muscle [25]. Of them, the cartilage rings are critical for maintaining the rigidity and luminal patency of the artificial trachea. Therefore, the development of biomimetic cartilage components with defined rigidity and elasticity is essential for the reconstruction and functionality of biomimetic trachea substitutes [26]. Currently, hydrogels offer significant advantages in artificial cartilage tissue reconstruction owing to their advantages in maintaining the phenotype and supporting the amplification of chondrocytes *in vitro* [27,28]. For cartilage bioengineering applications, sufficient hydrogel strength is particularly important, as it can maintain the shape of the cell-hydrogel

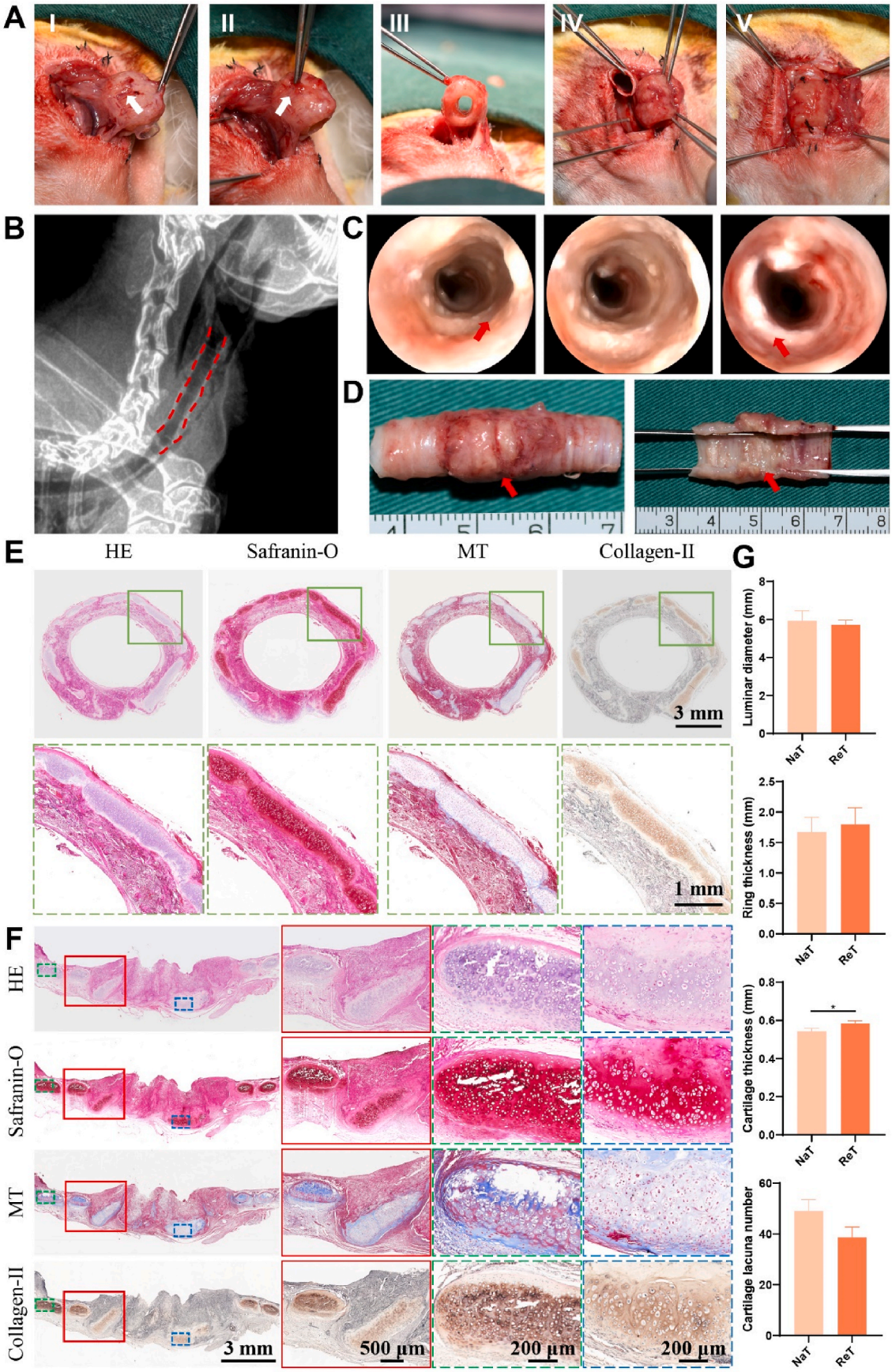

(caption on next page)

Fig. 9. Segmental tracheal reconstruction using biomimetic artificial tracheal grafts and treatment outcomes in a rabbit model. (A) Gross images of well-vascularized tracheal grafts with a pedicled muscle flap and silicon support (I and II). Luminal patency of artificial tracheal grafts after removing the silicon tube (III). Tracheal resection (IV). The engineered trachea was trimmed, and end-to-end anastomosis of the reconstructed tracheal grafts with the host remnant trachea stump was performed (V). White arrow: small blood vessels around the engineered trachea. (B) X-ray images of repaired tracheal defects 4 weeks after surgery. The red dotted line represents tracheal lumen patency. (C) Tracheoscopy images of the *in situ* reconstructed trachea 4 weeks after surgery. Red arrows indicate the proximal and distal anastomoses of the engineered trachea. (D) Gross view of the reconstructed trachea 4 weeks after surgery. Red arrows indicate the regenerated trachea. (E) Cross-sectioned view of the rabbit trachea stained with HE, safranin-O, Masson's trichrome (MT), and type II collagen. (F) Longitudinally sectioned rabbit trachea stained with HE, safranin-O, MT, and type II collagen. (G) Morphological and histological quantitative analysis of regenerated cartilage compared to native rabbit trachea cartilage (n = 3 independent samples, *: $p < 0.05$).

construct and reduce the *in vitro* culturing time needed to achieve upgrading mechanical properties. Various methods, such as a double crosslinking strategy and double-network hydrogel, have been adopted to generate high-strength hydrogels [29,30]. However, achieving hydrogels with satisfactory mechanical properties often comes at the expense of a high cross-linking density and small average pore size in the hydrogel networks, leading to limited cellular infiltration and nutrient exchange and consequently poor cartilage tissue regeneration [31].

Native cartilage ECM consists of an integrated fibrous protein network and a proteoglycan-based ground (hydrogel) substance, both of which are important for maintaining the mechanical and functional properties of tracheal cartilage tissue [32]. Inspired by the structural characteristics of natural cartilage tissue, we designed a highly biomimetic hydrogel that incorporates fibrous structures into traditional hydrogel architectures. As the native fibrous structure mimics the collagen fibers of native cartilage, BC nanofibers were chosen to enhance the mechanical properties of the hydrogel. However, the chemical inertness and non-biodegradability of BC greatly limit its application in tissue engineering. To address this issue, sOBC nanofibers were introduced into GelMA hydrogel to prepare the nanofiber-hydrogel composite, leveraging its degradation and bioactive surface for the loading of functional biomolecules like TGF-β [33]. The introduction of sOBC nanofibers had minimal impact on the gelling performance of the GelMA hydrogel. Importantly, the resulting nanofiber-hydrogel composite exhibited excellent elastic mechanical properties, as it could be repeatedly compressed at a strain of 1000 times without significant plastic deformation or structural damage. With a larger aspect ratio, the introduction of sOBC into the GelMA hydrogel resulted in a greater formation of hydrogen bonds between the nanofibers and hydrogel molecular chains, which helped maintain the structural stability of the hydrogel and improve its mechanical characteristics [10,34]. Therefore, a cartilage structure-inspired biomimetic hydrogel was fabricated by incorporating sOBC nanofibers into a GelMA hydrogel. Furthermore, native cartilage is a highly specialized tissue composed of chondrocytes and a cartilage-specific ECM, which consists of negatively charged GAGs interpenetrating a collagenous fibrillar network [35]. By encapsulating chondrocytes in our fabricated nanofiber-hydrogel composite, nascent immature cartilage tissue was constructed to a certain extent.

Another major challenge in constructing artificial tracheal cartilage is the limited availability of chondrocytes during biopsy. Owing to the loss of their distinctive phenotypes and functionalities after serial passage for chondrocytes during lengthy *in vitro* monolayer culture, it is difficult to simultaneously meet the density required for optimal tissue engineering and retain high-quality chondrocytes [28]. Previous research has shown that the initial seeding densities for cell-hydrogel constructs range from 10 to 130 million cells/mL, and a high seeding density is required to reach native cartilage properties, which is difficult to achieve in practice [13,36,37]. Otherwise, a prolonged *in vitro* culture time is required for cell-hydrogel constructs with low seeding density (20×10^6 cells/mL) to achieve satisfactory mechanical properties and functional cartilage tissue formation, similar to high seeding density (40×10^6 cells/mL); however, this may still be accompanied by the drawback of inferior ECM deposition [38]. Furthermore, the ability of chondrocytes to produce a cartilaginous matrix following expansion has been shown to decrease as the expansion number increases [39]. Therefore, constructing neocartilage tissue faces the challenge of scarce cell sources and the deteriorating post-expansion chondrogenic potential of chondrocytes.

To address this issue, we constructed a dual growth factor release system in a nanofiber-hydrogel composite to maximize the use of limited chondrocyte resources and obtain high-quality artificial tracheal cartilage. The hydrogel system with a dual growth factor release profile, consisting of a high concentration of FGF initially followed by a decreasing concentration over time and a slower/sustained release of TGF-β, is realized by immobilizing FGF in GelMA hydrogel and TGF-β within sOBC nanofibers. Due to the synergistic effect of FGF and TGF-β during the initial proliferation stage, the BTGF hydrogel exhibited the highest cell proliferation rates, and showed great potential in reducing the seeding density of the chondrocytes [14,40]. The burst release of FGF during initial proliferation can achieve the expansion of chondrocytes in a 3D environment and circumvents the dedifferentiation of monolayer expansion [41]. Furthermore, the sustained release of TGF-β further modulates the chondrocytes' ability to re-enter the chondral lineage-specific differentiation program. Importantly, the quality of the regenerated neo-cartilage tissue by the BTGF hydrogel with a seeding density of 20 million cells/mL was equivalent to that with a seeding density of over 40 million cells/mL by the BG hydrogel, as evidenced by the relatively equivalent abundance of GAG and type II collagen matrix deposition. Thus, the BTGF hydrogel reduces the required number of donor chondrocytes and provides superior augmentation of cell function to differentiate and produce cartilage-specific ECM in response to chondrogenic stimuli. Using the BTGF hydrogel, functional biomimetic tracheal cartilage rings were successfully fabricated after *in vitro* and *in vivo* cultures.

Furthermore, we investigated the feasibility of using neo-cartilage tissue to construct artificial tracheas. An interdigitated arrangement of chondral and BC fibrous rings was constructed to build a tubular trachea replacement. After implantation within the muscle pedicles, the surrounding connective tissue is integrated into the transplanted artificial tracheas. Furthermore, the connective ring surrounding the artificial trachea and the adjacent cartilage tubes formed a vascularized network, which is necessary for the maturation of the cartilage tissue and epithelialization of the artificial trachea after implantation. Owing to the successful regeneration of ring-shaped cartilage tissue resembling native tracheal cartilage after *in vivo* maturation, the constructed tissue-engineered tracheal substitutes exhibited sufficient strength after removing the silicon stent [42]. The tissue-engineered tracheal substitutes were used for tracheal defect repair and exhibited satisfactory repair outcomes. Four weeks after transplantation, the luminal surface of the reconstructed trachea from the anastomotic site to the other side was smooth, and the tracheal lumen was patent. Histologically, the tracheal cartilage equivalents based on the BTGF hydrogel system fully formed mature tracheal cartilage tissue with high morphological ring fidelity, abundant cartilage-specific ECM deposition, and mature cartilage lacunae formation.

Although our study demonstrated the feasibility of using biomimetic nanofiber-hydrogel composites to construct transplantable neo-cartilage tissue for regenerating TETG and repairing long-segment tracheal defects, it has few limitations. First, although using chondrocytes to construct the tracheal cartilage is efficient, a significant drawback is that constructing a human-sized artificial trachea still requires a certain number of chondrocytes, which are difficult to obtain in clinical

practice. One promising substitute cell source is mesenchymal stem cells (MSCs) [42]. The potential of the designed hydrogel to induce the chondrogenic differentiation of MSCs and form neo-cartilage tissues will be investigated further. Second, although the blood supply to the implanted trachea was achieved in the current study, epithelialization of the artificial trachea remains unclear. Regeneration of the tracheal epithelium depends on the innate reparative capacity of the host's epithelium [43]. In future studies, we will further integrate the regeneration and reconstruction of epithelial structural units into tissue-engineered tracheas established using existing cartilage units.

5. Conclusion

In conclusion, inspired by the native cartilage structure, we developed a unique nanofiber-hydrogel composite that mimics the microarchitecture and mechanical properties of cartilage tissue. Based on this composite, we designed an innovative biomaterial system featuring high proliferative and a typical cartilage ECM-production ability to enable faster translational cartilage analogs production. The biomaterial platform, with the dual growth factor release profile, effectively regulates chondrocyte behavior and provides a step-wise mature of neo-cartilage tissue. After the *in vitro* culture and *in vivo* implantation, high-quality neo-cartilage regeneration was achieved by encapsulating a relatively low cell density within the biomaterial system, as evidenced by the native lacunae structure surrounded by an abundant territorial matrix. Furthermore, the regenerated ring-shaped neo-cartilage tissues were successfully applied for the construction of artificial trachea and repair of tracheal defects. Overall, we developed a highly biomimetic nanofiber-hydrogel composite with a fully defined tailor-made strategy to achieve efficient regeneration of mature cartilage analogs for reconstructing artificial trachea substitutes and repairing tracheal defects.

CRediT authorship contribution statement

Yaqiang Li: Writing – review & editing, Writing – original draft, Formal analysis, Conceptualization. **Xiaowei Xun:** Software, Formal analysis. **Liang Duan:** Funding acquisition. **Erji Gao:** Writing – original draft, Software. **Jiaxin Li:** Writing – original draft, Data curation. **Lei Lin:** Project administration, Methodology, Investigation. **Xinping Li:** Supervision, Software, Resources. **Aijuan He:** Funding acquisition, Writing – review & editing. **Haiyong Ao:** Investigation, Data curation. **Yong Xu:** Funding acquisition. **Huitang Xia:** Resources, Investigation, Funding acquisition, Data curation.

Ethics approval and consent to participate

All animal care, housing conditions, and experimental protocols were strictly in compliance with the Guide for the Care and Use of Laboratory Animals of the Shanghai Pulmonary Hospital Ethics Committee, ensuring both ethical treatment of the animals and scientific rigor in our study (K19-080Y).

Declaration of competing interest

The authors declare no competing interests.

Acknowledgements

This work was supported by National Key R&D Program of China (Grant No. 2024YFA1107800), National Natural Science Foundation of China (Grant Nos. 82302395, 82160355, and 82172105), Shanghai Sailing Program (Grant Nos. 22YF1423200 and 22YF1437400), Shanghai Rising-Star Program (Grant No. 24QB2704800), Taishan Scholar Program of Shandong Province (Grant No. tsqn202312359) and Young Elite Scientists Sponsorship Program by CAST (Grant No. 2023QNRC001). We would like to thank Editage (www.editage.cn) for English language editing.

Appendix A. Supplementary data

Supplementary data to this article can be found online at https://doi.org/10.1016/j.bioactmat.2025.01.007.

References

[1] F. Kolb, F. Simon, R. Gaudin, B. Thierry, S. Mussot, L. Dupic, J.L. Coste, N. Leboulanger, F. Denoyelle, V. Couloigner, E.N. Garabedian, 4-Year follow-up in a child with a total autologous tracheal replacement, N. Engl. J. Med. 378 (14) (2018) 1355–1357, https://doi.org/10.1056/NEJMc1800095.

[2] J.H. Park, J.Y. Park, I.C. Nam, S.H. Hwang, C.S. Kim, J.W. Jung, J. Jang, H. Lee, Y. Choi, S.H. Park, S.W. Kim, D.W. Cho, Human turbinate mesenchymal stromal cell sheets with bellows graft for rapid tracheal epithelial regeneration, Acta Biomater. 25 (2015) 56–64, https://doi.org/10.1016/j.actbio.2015.07.014.

[3] K. Kobayashi, T. Suzuki, Y. Nomoto, Y. Tada, M. Miyake, A. Hazama, I. Wada, T. Nakamura, K. Omori, A tissue-engineered trachea derived from a framed collagen scaffold, gingival fibroblasts and adipose-derived stem cells, Biomaterials 31 (18) (2010) 4855–4863, https://doi.org/10.1016/j.biomaterials.2010.02.027.

[4] Y. Sun, Y. Huo, X. Ran, H. Chen, Q. Pan, Y. Chen, Y. Zhang, W. Ren, X. Wang, G. Zhou, Y. Hua, Instant tracheal reconstruction using 3D-bioprinted C-shape biomimetic trachea based on tissue-specific matrix hydrogels, Bioact. Mater. 32 (2024) 52–65, https://doi.org/10.1016/j.bioactmat.2023.09.011.

[5] S. Dharmadhikari, L. Liu, K. Shontz, M. Wiet, A. White, A. Goins, H. Akula, J. Johnson, S.D. Reynolds, C.K. Breuer, T. Chiang, Deconstructing tissue engineered trachea: assessing the role of synthetic scaffolds, segmental replacement and cell seeding on graft performance, Acta Biomater. 102 (2020) 181–191, https://doi.org/10.1016/j.actbio.2019.11.008.

[6] P.S. Wiggenhauser, J.T. Schantz, N. Rotter, Cartilage engineering in reconstructive surgery: auricular, nasal and tracheal engineering from a surgical perspective, Regen. Med. 12 (3) (2017) 303–314, https://doi.org/10.2217/rme-2016-0160.

[7] K. Yue, G. Trujillo-de Santiago, M.M. Alvarez, A. Tamayol, N. Annabi, A. Khademhosseini, Synthesis, properties, and biomedical applications of gelatin methacryloyl (GelMA) hydrogels, Biomaterials 73 (2015) 254–271, https://doi.org/10.1016/j.biomaterials.2015.08.045.

[8] M.A. Sakr, K. Sakthivel, T. Hossain, S.R. Shin, S. Siddiqua, J. Kim, K. Kim, Recent trends in gelatin methacryloyl nanocomposite hydrogels for tissue engineering, J. Biomed. Mater. Res., Part A 110 (3) (2022) 708–724, https://doi.org/10.1002/jbm.a.37310.

[9] J. Li, G. Chen, X. Xu, P. Abdou, Q. Jiang, D. Shi, Z. Gu, Advances of injectable hydrogel-based scaffolds for cartilage regeneration, Regen. Biomaterials 6 (3) (2019) 129–140, https://doi.org/10.1093/rb/rbz022.

[10] S. Chayanun, A.A. Soufivand, J. Faber, S. Budday, B. Lohwongwatana, A. R. Boccaccini, Reinforcing tissue-engineered cartilage: nanofibrillated cellulose enhances mechanical properties of alginate dialdehyde–gelatin hydrogel, Adv. Eng. Mater. 26 (4) (2023) 2300641, https://doi.org/10.1002/adem.202300641.

[11] A. Karimizade, E. Hasanzadeh, M. Abasi, S.E. Enderami, E. Mirzaei, N. Annabi, A. Mellati, Collagen short nanofiber-embedded chondroitin sulfate-hyaluronic acid nanocomposite: a cartilage-mimicking in situ-forming hydrogel with fine-tuned properties, Int. J. Biol. Macromol. 266 (Pt 2) (2024) 131051, https://doi.org/10.1016/j.ijbiomac.2024.131051.

[12] J.C. Schagemann, E.H. Mrosek, R. Landers, H. Kurz, C. Erggelet, Morphology and function of ovine articular cartilage chondrocytes in 3-d hydrogel culture, Cells Tissues Organs 182 (2) (2006) 89–97, https://doi.org/10.1159/000093063.

[13] A.D. Cigan, B.L. Roach, R.J. Nims, A.R. Tan, M.B. Albro, A.M. Stoker, J.L. Cook, G. Vunjak-Novakovic, C.T. Hung, G.A. Ateshian, High seeding density of human chondrocytes in agarose produces tissue-engineered cartilage approaching native mechanical and biochemical properties, J. Biomech. 49 (9) (2016) 1909–1917, https://doi.org/10.1016/j.jbiomech.2016.04.039.

[14] I.M. Khan, L. Francis, P.S. Theobald, S. Perni, R.D. Young, P. Prokopovich, R. S. Conlan, C.W. Archer, In vitro growth factor-induced bio engineering of mature articular cartilage, Biomaterials 34 (5) (2013) 1478–1487, https://doi.org/10.1016/j.biomaterials.2012.09.076.

[15] Y. Wen, Y. Chen, W. Wu, H. Zhang, Z. Peng, X. Yao, X. Zhang, W. Jiang, Y. Liao, Y. Xie, X. Shen, H. Sun, J. Hu, H. Liu, X. Chen, J. Chen, H. Ouyang, Hyperplastic human macromass cartilage for joint regeneration, Adv. Sci. 10 (26) (2023) e2301833, https://doi.org/10.1002/advs.202301833.

[16] Y. Li, X. Xun, Y. Xu, A. Zhan, E. Gao, F. Yu, Y. Wang, H. Luo, C. Yang, Hierarchical porous bacterial cellulose scaffolds with natural biomimetic nanofibrous structure and a cartilage tissue-specific microenvironment for cartilage regeneration and repair, Carbohydr. Polym. 276 (2022) 118790, https://doi.org/10.1016/j.carbpol.2021.118790.

[17] X. Xun, Y. Li, X. Zhu, Q. Zhang, Y. Lu, Z. Yang, Y. Wan, F. Yao, X. Deng, H. Luo, Fabrication of robust, shape recoverable, macroporous bacterial cellulose scaffolds for cartilage tissue engineering, Macromol. Biosci. 21 (11) (2021) e2100167, https://doi.org/10.1002/mabi.202100167.

[18] E. Luz, P.H.S. Chaves, L.A.P. Vieira, S.F. Ribeiro, M.F. Borges, F.K. Andrade, C. R. Muniz, A. Infantes-Molina, E. Rodriguez-Castellon, M.F. Rosa, R.S. Vieira, In vitro degradability and bioactivity of oxidized bacterial cellulose-hydroxyapatite composites, Carbohydr. Polym. 237 (2020) 116174, https://doi.org/10.1016/j.carbpol.2020.116174.

[19] C. Li, Y.X. Zhu, Y. Yang, W. Miao, X. Shi, K.F. Xu, Z.H. Li, H. Xiao, F.G. Wu, Bioinspired multifunctional cellulose film: in situ bacterial capturing and killing for managing infected wounds, Bioact. Mater. 36 (2024) 595–612, https://doi.org/10.1016/j.bioactmat.2024.06.031.

[20] J. He, Y. Sun, Q. Gao, C. He, K. Yao, T. Wang, M. Xie, K. Yu, J. Nie, Y. Chen, Y. He, Gelatin methacryloyl hydrogel, from standardization, performance, to biomedical application, Adv. Healthcare Mater. 12 (23) (2023) e2300395, https://doi.org/10.1002/adhm.202300395.

[21] Y. Li, Y. Liu, X. Xun, W. Zhang, Y. Xu, D. Gu, Three-dimensional porous scaffolds with biomimetic microarchitecture and bioactivity for cartilage tissue engineering, ACS Appl. Mater. Interfaces 11 (40) (2019) 36359–36370, https://doi.org/10.1021/acsami.9b12206.

[22] H. Xia, D. Zhao, H. Zhu, Y. Hua, K. Xiao, Y. Xu, Y. Liu, W. Chen, Y. Liu, W. Zhang, W. Liu, S. Tang, Y. Cao, X. Wang, H.H. Chen, G. Zhou, Lyophilized scaffolds fabricated from 3D-printed photocurable natural hydrogel for cartilage regeneration, ACS Appl. Mater. Interfaces 10 (37) (2018) 31704–31715, https://doi.org/10.1021/acsami.8b10926.

[23] A. He, H. Xia, K. Xiao, T. Wang, Y. Liu, J. Xue, D. Li, S. Tang, F. Liu, X. Wang, W. Zhang, W. Liu, Y. Cao, G. Zhou, Cell yield, chondrogenic potential, and regenerated cartilage type of chondrocytes derived from ear, nasoseptal, and costal cartilage, J. Tissue Eng. Regen. Med. 12 (4) (2018) 1123–1132, https://doi.org/10.1002/term.2613.

[24] S.P. Grogan, A. Barbero, V. Winkelmann, F. Rieser, J.S. Fitzsimmons, S. O'Driscoll, I. Martin, P. Mainil-Varlet, Visual histological grading system for the evaluation of in vitro-generated neocartilage, Tissue Eng. 12 (8) (2006) 2141–2149, https://doi.org/10.1089/ten.2006.12.2141.

[25] K. Kishimoto, M. Tamura, M. Nishita, Y. Minami, A. Yamaoka, T. Abe, M. Shigeta, M. Morimoto, Synchronized mesenchymal cell polarization and differentiation shape the formation of the murine trachea and esophagus, Nat. Commun. 9 (1) (2018) 2816, https://doi.org/10.1038/s41467-018-05189-2.

[26] C.K. Tsao, C.Y. Ko, S.R. Yang, C.Y. Yang, E.M. Brey, S. Huang, I.M. Chu, M. H. Cheng, An ectopic approach for engineering a vascularized tracheal substitute, Biomaterials 35 (4) (2014) 1163–1175, https://doi.org/10.1016/j.biomaterials.2013.10.055.

[27] Z. Miao, Z. Lu, H. Wu, H. Liu, M. Li, D. Lei, L. Zheng, J. Zhao, Collagen, agarose, alginate, and Matrigel hydrogels as cell substrates for culture of chondrocytes in vitro: a comparative study, J. Cell. Biochem. 119 (10) (2018) 7924–7933, https://doi.org/10.1002/jcb.26411.

[28] Y. Ling, W. Zhang, P. Wang, W. Xie, W. Yang, D.A. Wang, C. Fan, Three-dimensional (3D) hydrogel serves as a platform to identify potential markers of chondrocyte dedifferentiation by combining RNA sequencing, Bioact. Mater. 6 (9) (2021) 2914–2926, https://doi.org/10.1016/j.bioactmat.2021.02.018.

[29] Y. Zhao, Z.S. Zhu, J. Guan, S.J. Wu, Processing, mechanical properties and bio-applications of silk fibroin-based high-strength hydrogels, Acta Biomater. 125 (2021) 57–71, https://doi.org/10.1016/j.actbio.2021.02.018.

[30] J.P. Gong, Y. Katsuyama, T. Kurokawa, Y. Osada, Double-network hydrogels with extremely high mechanical strength, Adv. Mater. 15 (14) (2003) 1155–1158, https://doi.org/10.1002/adma.200304907.

[31] S. Khetan, M. Guvendiren, W.R. Legant, D.M. Cohen, C.S. Chen, J.A. Burdick, Degradation-mediated cellular traction directs stem cell fate in covalently crosslinked three-dimensional hydrogels, Nat. Mater. 12 (5) (2013) 458–465, https://doi.org/10.1038/nmat3586.

[32] J. Coburn, M. Gibson, P.A. Bandalini, C. Laird, H.Q. Mao, L. Moroni, D. Seliktar, J. Elisseeff, Biomimetics of the extracellular matrix: an integrated three-dimensional fiber-hydrogel composite for cartilage tissue engineering, Smart Struct. Syst. 7 (3) (2011) 213–222, https://doi.org/10.12989/sss.2011.7.3.213.

[33] Z. Wei, F.F. Hong, Z. Cao, S.Y. Zhao, L. Chen, In situ fabrication of nerve growth factor encapsulated chitosan nanoparticles in oxidized bacterial nanocellulose for rat sciatic nerve regeneration, Biomacromolecules 22 (12) (2021) 4988–4999, https://doi.org/10.1021/acs.biomac.1c00947.

[34] Q. Wang, Ö. Karadas, J.M. Rosenholm, C. Xu, T. Näreoja, X. Wang, Bioprinting macroporous hydrogel with aqueous two-phase emulsion-based bioink: in vitro mineralization and differentiation empowered by phosphorylated cellulose nanofibrils, Adv. Funct. Mater. 34 (29) (2024) 2400431, https://doi.org/10.1002/adfm.202400431.

[35] F.A. Formica, E. Ozturk, S.C. Hess, W.J. Stark, K. Maniura-Weber, M. Rottmar, M. Zenobi-Wong, A bioinspired ultraporous nanofiber-hydrogel mimic of the cartilage extracellular matrix, Adv. Healthcare Mater. 5 (24) (2016) 3129–3138, https://doi.org/10.1002/adhm.201600867.

[36] R.L. Mauck, C.C. Wang, E.S. Oswald, G.A. Ateshian, C.T. Hung, The role of cell seeding density and nutrient supply for articular cartilage tissue engineering with deformational loading, Osteoarthritis Cartilage 11 (12) (2003) 879–890, https://doi.org/10.1016/j.joca.2003.08.006.

[37] Y. Xu, Y. Xu, B. Bi, M. Hou, L. Yao, Q. Du, A. He, Y. Liu, C. Miao, X. Liang, X. Jiang, G. Zhou, Y. Cao, A moldable thermosensitive hydroxypropyl chitin hydrogel for 3D cartilage regeneration in vitro and in vivo, Acta Biomater. 108 (2020) 87–96, https://doi.org/10.1016/j.actbio.2020.03.039.

[38] W. Sun, Y. Yang, L. Wang, H. Tang, L. Zhang, Y. She, X. Xiao, X. Hu, Q. Feng, C. Chen, Utilization of an acellular cartilage matrix-based photocrosslinking hydrogel for tracheal cartilage regeneration and circumferential tracheal repair, Adv. Funct. Mater. 32 (2022) 22021257, https://doi.org/10.1002/adfm.202201257.

[39] M.K. Murphy, D.J. Huey, A.J. Reimer, J.C. Hu, K.A. Athanasiou, Enhancing post-expansion chondrogenic potential of costochondral cells in self-assembled neocartilage, PLoS One 8 (2) (2013) e56983, https://doi.org/10.1371/journal.pone.0056983.

[40] M. Jakob, O. Demarteau, D. Schafer, B. Hintermann, W. Dick, M. Heberer, I. Martin, Specific growth factors during the expansion and redifferentiation of adult human articular chondrocytes enhance chondrogenesis and cartilaginous tissue formation in vitro, J. Cell. Biochem. 81 (2) (2001) 368–377, https://doi.org/10.1002/1097-4644(20010501)81:2<368::aid-jcb1051>3.0.co;2-j.

[41] A.R. Armiento, M. Alini, M.J. Stoddart, Articular fibrocartilage - why does hyaline cartilage fail to repair? Adv. Drug Deliv. Rev. 146 (2019) 289–305, https://doi.org/10.1016/j.addr.2018.12.015.

[42] R. Machino, K. Matsumoto, D. Taniguchi, T. Tsuchiya, Y. Takeoka, Y. Taura, M. Moriyama, T. Tetsuo, S. Oyama, K. Takagi, T. Miyazaki, G. Hatachi, R. Doi, K. Shimoyama, N. Matsuo, N. Yamasaki, K. Nakayama, T. Nagayasu, Replacement of rat tracheas by layered, trachea-like, scaffold-free structures of human cells using a bio-3D printing system, Adv. Healthcare Mater. 8 (7) (2019) e1800983, https://doi.org/10.1002/adhm.201800983.

[43] B. Gao, H. Jing, M. Gao, S. Wang, W. Fu, X. Zhang, X. He, J. Zheng, Long-segmental tracheal reconstruction in rabbits with pedicled Tissue-engineered trachea based on a 3D-printed scaffold, Acta Biomater. 97 (2019) 177–186, https://doi.org/10.1016/j.actbio.2019.07.043.